Electronic Supplementary Information (ESI)

Long-wavelength triggered iridium(III) complex nanoparticles for photodynamic therapy against hypoxic cancer

Shengnan Liu [a], *Ziwei Wang* [a], *Zihan Wu* [a], *Haoran Chen* [b], *Dongxia Zhu** [a], *Gungzhe Li** [c], *Mingming Yan* [c], *Martin R. Bryce** [d] *and Yulei Chang** [b]

[a] Dr. S. Liu, Dr. Z. Wang, Mr. Z. Wu, and Prof. D. Zhu

Key Laboratory of Nanobiosensing and Nanobioanalysis at Universities of Jilin Province, Department of Chemistry, Northeast Normal University, 5268 Renmin Street, Changchun, Jilin Province 130024, P.R. China.

*E-mail: zhudx047@nenu.edu.cn

[b] Dr. H. Chen, Prof. Y. Chang

State Key Laboratory of Luminescence and Applications, Changchun Institute of Optics, Fine Mechanics and Physics, Chinese Academy of Sciences, Changchun Jilin Province 130033, P.R. China.

*E-mail: yuleichang@ciomp.ac.cn

[c] Prof. G. Li

Jilin Provincial Science and Technology Innovation Center of Health Food of Chinese Medicine, Changchun University of Chinese Medicine, Changchun, Jilin Province 130117, P. R. China.

E-mail: 1993008106@qq.com

[d] Prof. Martin R. Bryce

Department of Chemistry, Durham University, Durham, DH1 3LE, UK.

*E-mail: m.r.bryce@durham.ac.uk

Table of Contents

Experimental section

Materials and Instruments

Materials for organic synthesis were purchased from the Energy Chemical Company. Chlorin e6 (Ce6), Rose Bengal (RB), zinc phthalocyanine (ZnPc), hematoporphyrin derivative (HpD), 2',7'-dichlorodihydrofluorescein (DCFH), 2-[10-(2,2-dicarboxyethyl)anthracen-9-yl]methylpropanedioic acid (ABDA), 5,5-dimethyl-1-pyrroline-*N*-oxide (DMPO), 2,2,6,6-tetramethylpiperidine (TEMP) and dihydrorhodamine 123 (DHR 123) were purchased from Aladdin Chemical Company. RPMI Medium 1640 was purchased from Solarbio Life Science Company. Fetal bovine serum (FBS) was purchased from Sigma-Aldrich. 3-(4,5-dimethyl-2-thiazolyl)-2,5-diphenyltetrazolium bromide (MTT), 2,7-dichlorofluorescence diacetate (DCFH-DA) and the cell viability (live dead cell staining) assay kit were purchased from Shanghai Beyotime Biotechnology Co., mPEG-SC-2000 (PEG-NHS-2000) was purchased from Xiamen Sinopeg Biotechnology Co.

^{1}H NMR spectra were recorded at 25 °C on a Varian 500 MHz spectrometer in commercially available deuterated solvents and referenced internally to the residual solvent proton resonances. UV-vis absorption spectra were recorded on a Shimadzu UV-3100 spectrophotometer. The photoluminescence spectra were recorded on an Edinburgh-FLS980 spectrofluorimeter (for λ_{ex} = 450 nm) and an Ocean Optics Maya-2000 spectrofluorimeter (for λ_{ex} = 655 nm). The lifetimes (τ) (under N_2) and photoluminescence quantum yields (Φ) (under air) were recorded on an Edinburgh FLS920 spectrofluorimeter at room temperature. Transmission electron microscopy (TEM) images were taken by a TECNAI F20 microscope. Diameter and diameter distribution of the nanoparticles were determined by a Malvern Zetasizer Nano instrument for dynamic light scattering (DLS). Confocal laser scanning microscopy (CLSM) images were taken using a ZeissLSM 700 (Zurich, Switzerland).

Synthesis of the Schiff base (Schiff-NH_2)

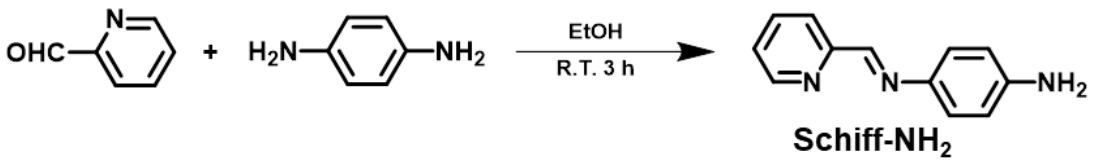

Scheme S1. Synthetic route for **Schiff-NH2**.

According to the literature method,[1] *p*-phenylenediamine (648 mg，6.0 mmol) was dissolved in EtOH (30 mL), stirred at room temperature for 30 min. 2-pyridinecarboxaldehyde 642 mg (6.0 mmol) was dissolved in EtOH (5 mL), dropped into the p-phenylenediamine solution at a rate of 1 mL per 30 min. After the addition was completed, the mixture was stirred at room temperature for an additional 1 h to form a yellow precipitate. Then the precipitate was collected through filtering, washed with ethanol and petroleum ether, and dried at 68 ℃ to obtain **Schiff-NH2**. Yield, 90%. ^{1}H NMR (500 MHz, DMSO-d_6, δ[ppm]): 8.57 (d, J = 4.6 Hz, 1H), 8.49 (s, 1H), 8.00 (d, J = 7.9 Hz, 1H), 7.80 (t, J = 7.6 Hz, 1H), 7.37-7.33 (m, 1H), 7.13 (d, J = 8.3 Hz, 2H), 6.52 (d, J = 8.3 Hz, 2H), 5.31 (s, 2H) (Fig. S1).

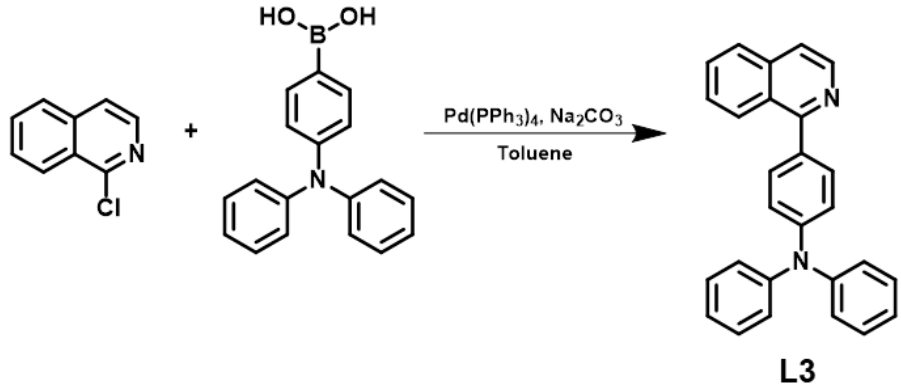

Scheme S2. Synthetic route for **C^N ligand L3**.

Synthesis of the C^N ligand L3

According to the literature method,[2, 3] 1-chloroisoquinoline (248 mg, 1.5 mmol) and 4-boronic acid triphenylamine (486 mg, 1.7 mmol) were dissolved in toluene (20 mL) and tetrakis(triphenylphosphine)palladium(0) (90 mg, 0.08 mmol) was added as a catalyst. Sodium carbonate (10 mL of 2 mol L^{-1} solution) was added and the mixture was refluxed for 48 h under N_2 protection. The mixture was then left to cool and

extracted with dichloromethane. The organic phase was dried over anhydrous $MgSO_4$, and the crude product was purified by silica gel column chromatography (dichloromethane/petroleum ether, 10/3 v/v) to obtain pure yellow solid **L3**. Yield, 52%. ^{1}H NMR (500 MHz, $CDCl_3$, δ [ppm]): 8.61 (d, *J* = 5.4 Hz, 1H), 8.27 (d, *J* = 8.4 Hz, 1H), 7.90 (d, *J* = 7.6 Hz, 1H), 7.73 (t, *J* = 7.8 Hz, 1H), 7.66-7.56 (m, 4H), 7.34-7.26 (m, 4H), 7.27-7.15 (m, 6H), 7.07 (t, J = 7.4 Hz, 2H).

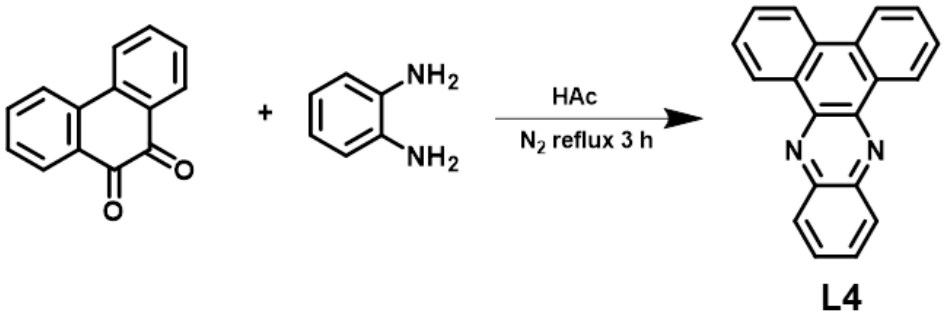

Scheme S3. Synthetic route for **C^N ligand L4**.

Synthesis of the C^N ligand L4

As shown in Scheme S3,[4] phenanthrenequinone (624 mg, 3mmol) and o-phenylenediamine (324 mg,3mmol) were dissolved in acetic acid (10 mL), and the mixture refluxed for 3 h under N_2. After the reaction was complete, the mixture was poured into ice water (500 mL) to form a clear light-yellow precipitate. The precipitate was filtered and then washed with a large amount of water and ethanol and dried at 68 ℃ to obtain a light-yellow ligand **L4**. Yield, 92%. ^{1}H NMR (500 MHz, $CDCl_3$, δ [ppm]): 9.45 (dd, *J* = 7.9, 1.2 Hz, 1H), 8.58 (d, *J* = 7.9 Hz, 1H), 8.38 (dd, *J* = 6.5, 3.4 Hz, 1H), 7.87 (dd, *J* = 6.5, 3.4 Hz, 1H), 7.83-7.76 (m, 2H) (Fig. S2).

Synthesis of the C^N ligand L5

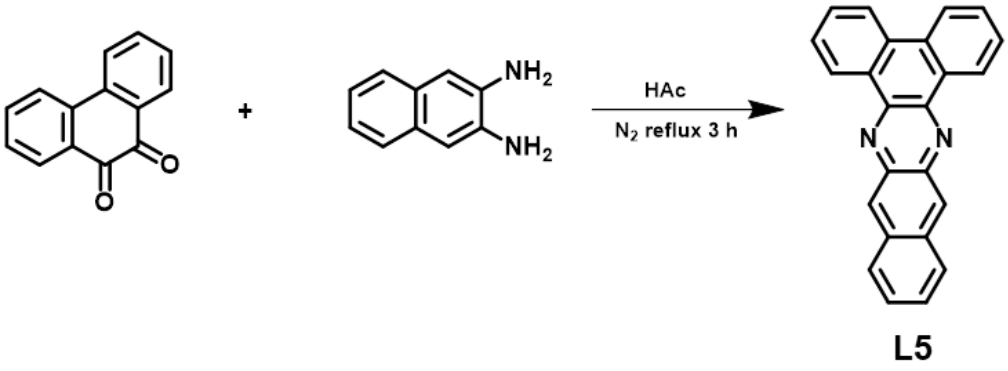

Scheme S4. Synthetic route for **C^N ligand L5**.

As shown in Scheme S4, phenanthrenequinone (624 mg, 3 mmol) and 2,3-diaminonaphthalene (474 mg, 3 mmol) were dissolved in acetic acid (15 mL). After the reaction was complete, the mixture was poured into ice water (500 mL) to form a yellow precipitate. The precipitate was filtered and then washed with a large amount of water and ethanol and dried at 68 ℃ to obtain yellow ligand **L5**. Yield, 89%. ^{1}H NMR (500 MHz, $CDCl_3$, δ [ppm]): 9.36 (dd, *J* = 7.9, 1.3 Hz, 1H), 8.87 (s, 1H), 8.46 (d, *J* = 7.9 Hz, 1H), 8.13 (dd, *J* = 6.4, 3.2 Hz, 1H), 7.75-7.72 (m, 1H), 7.68 (t, *J* = 7.0 Hz, 1H), 7.53 (dd, *J* = 6.6, 3.1 Hz, 1H) (Fig. S3).

Synthesis of the dichloro-bridged diiridium complex [Ir(C^N)$_2$Cl]$_2$

The C^N ligand (ppy, piq, L3, L4 and L5, 3 mmol) and iridium trichloride hydrate (352 mg, 1 mmol) were dissolved in a mixture of 2-ethoxyethanol (30 mL) and water (10 mL) and reacted at 125 °C under an inert atmosphere of N_2 for 24 h. After cooling to room temperature, water was added to the solution and the precipitate was collected by filtration. The precipitate was washed with water and EtOH and dried at 68 °C to give dichloro-bridged diiridium complex **[Ir(C^N)$_2$Cl]$_2$**. This product was directly used in the subsequent reaction.

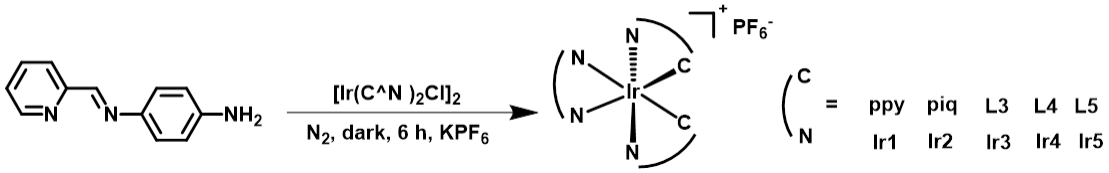

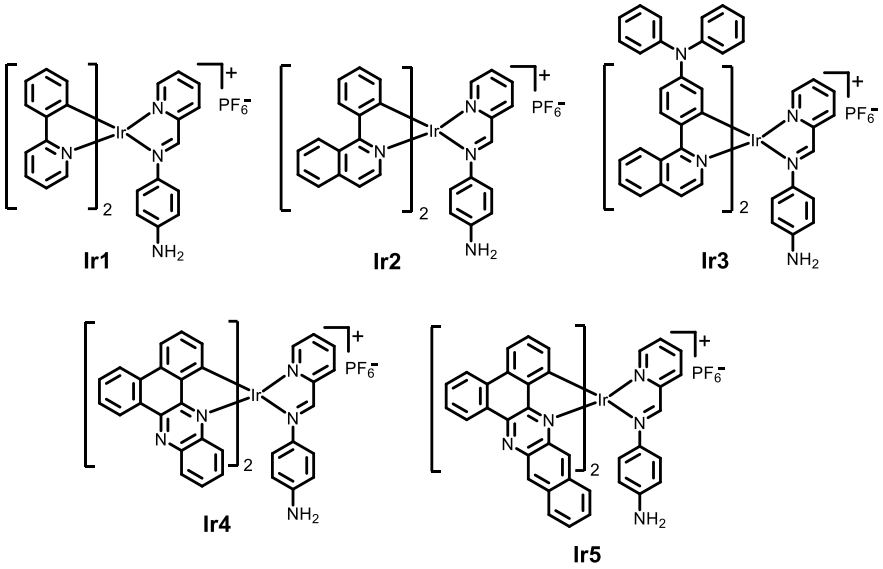

Scheme S5. Synthetic route for **Ir1-5** and their structures.

Synthesis of complexes Ir1-5

The prototypical synthetic route to $[Ir(C^N)_2(N^N)]^+$ complexes used here leads to a racemic mixture of Δ and Λ stereoisomers which were not separated.[5] The dichloro-bridged diiridium complex **$[Ir(C^N)_2Cl]_2$** (0.1 mmol) and **Schiff-NH_2** (39.4 mg, 0.2 mmol) in MeOH (30 ml) and CH_2Cl_2 (30 ml) was refluxed under an inert atmosphere of N_2 in the dark for 6 h. The red solution was then cooled to room temperature, and solid potassium hexafluorophosphate (370 mg, 20 mmol) was added to the solution. The mixture was stirred for 30 min at room temperature and the suspension was then filtered and the precipitate was washed with petroleum ether and dried to obtain crude product. The product was purified by silica gel column chromatography with CH_2Cl_2/MeOH (100/1, v/v) as eluent.

Ir1: red solid. Yield: 70%. ^{1}H NMR (500 MHz, DMSO-d_6 δ [ppm]): 9.42 (s, 1H), 8.39 (d, J = 7.8 Hz, 1H), 8.31 (d, J = 5.6 Hz, 1H), 8.28 (d, J = 8.2 Hz, 1H), 8.22 (td, J = 7.8, 1.3 Hz, 1H), 8.14 (d, J = 8.2 Hz, 1H), 7.98 (t, J = 7.8 Hz, 1H), 7.95 – 7.93 (m, 1H), 7.90 (d, J = 7.8 Hz, 1H), 7.73 – 7.70 (m, 2H), 7.65 – 7.62 (m, 1H), 7.52 (d, J = 5.5 Hz, 1H), 7.30 (t, J = 6.6 Hz, 1H), 7.23 (t, J = 6.6 Hz, 1H), 7.00 (t, J = 7.5 Hz, 1H), 6.87 (dd, J = 14.2, 7.0 Hz, 2H), 6.83 (d, J = 8.8 Hz, 2H), 6.78 (t, J = 7.4 Hz, 1H), 6.19 (d, J = 8.8 Hz, 2H), 6.08 (dd, J = 7.3, 5.0 Hz, 2H), 5.56 (s, 2H) (Fig. S4). ^{13}C NMR

(151 MHz, DMSO-d_6 δ [ppm]): 167.48, 166.96, 163.25, 156.71, 151.42, 150.93, 150.56, 150.00, 149.40, 149.25, 144.08, 143.94, 139.97, 139.21, 139.07, 137.32, 131.52, 131.12, 130.71, 130.20, 130.07, 129.43, 125.48, 125.12, 124.82, 124.62, 124.10, 122.92, 122.15, 120.56, 120.13, 113.32 (Fig. S5). MS:(MALDI-TOF) [m/z]: 698.19 (M^+) (Fig. S6). Calcd. for $C_{34}H_{27}F_6IrN_5P$: C 48.45, H, 3.23, N 8.31. Found: C 48.40, H 3.25, N 8.33.

Ir2: red solid. Yield: 64%. ^{1}H NMR (500 MHz, DMSO-d_6 δ [ppm]): 9.50 (s, 1H), 9.02 (d, J = 8.2 Hz, 1H), 8.83 (d, J = 8.6 Hz, 1H), 8.45 (d, J = 7.8 Hz, 1H), 8.37 (d, J = 8.0 Hz, 1H), 8.24 (d, J = 6.6 Hz, 2H), 8.16 (d, J = 8.0 Hz, 2H), 8.13 (d, J = 8.2 Hz, 1H), 7.92 (dd, J = 14.2, 7.6 Hz, 3H), 7.84 (t, J = 7.7 Hz, 1H), 7.78 (d, J = 6.4 Hz, 1H), 7.69 (d, J = 6.5 Hz, 1H), 7.62 (t, J = 6.5 Hz, 1H), 7.57 (d, J = 5.2 Hz, 1H), 7.45 (d, J = 6.4 Hz, 1H), 7.13 (t, J = 7.7 Hz, 1H), 6.98 (t, J = 7.6 Hz, 1H), 6.91 (t, J = 7.4 Hz, 1H), 6.78 – 6.73 (m, 3H), 6.18-6.12 (m, 3H), 6.06 (d, J = 7.6 Hz, 1H), 5.54 (s, 2H) (Fig. S7). ^{13}C NMR (151 MHz, DMSO-d_6 δ [ppm]): 168.35, 167.97, 163.38, 156.55, 154.73, 152.80, 150.48, 150.03, 145.46, 145.36, 142.45, 141.01, 140.03, 137.16, 137.00, 136.92, 132.60, 132.47, 131.84, 131.65, 131.03, 130.61, 130.37, 130.24, 129.96, 129.63, 129.47, 128.25, 128.07, 126.83, 126.09, 125.81, 124.70, 122.92, 122.87, 122.32, 122.15, 113.27 (Fig. S8). MS:(MALDI-TOF) [m/z]: 798.22 (M^+) (Fig. S9). Calcd. for $C_{42}H_{31}F_6IrN_5P$: C 53.50, H, 3.31, N 7.43. Found: C 53.48, H 3.29, N 7.45.

Ir3: dark red solid. Yield: 53%. ^{1}H NMR (500 MHz, DMSO-d_6 δ [ppm]): 9.45 (s, 1H), 8.73 (d, J = 8.5 Hz, 1H), 8.68 (d, J = 8.6 Hz, 1H), 8.40 (d, J = 7.9 Hz, 1H), 8.23 (t, J = 8.4 Hz, 1H), 8.09 (d, J = 9.0 Hz, 1H), 8.02 (d, J = 9.0 Hz, 1H), 7.88 (dd, J = 13.3, 8.1 Hz, 2H), 7.81 (d, J = 7.3 Hz, 1H), 7.78 (d, J = 7.9 Hz, 1H), 7.76 – 7.72 (m, 5H), 7.16 (dd, J = 9.7, 6.6 Hz, 2H), 7.03 (t, J = 7.8 Hz, 9H), 6.88 (t, J = 8.5 Hz, 8H), 6.77 (d, J = 8.8 Hz, 2H), 6.69 (d, J = 7.7 Hz, 4H), 6.59 (ddd, J = 29.5, 8.8, 2.4 Hz, 2H), 6.36 (d, J = 8.8 Hz, 2H), 5.67 (s, 2H), 5.53 (d, J = 2.4 Hz, 1H), 5.47 (d, J = 2.4 Hz, 1H) (Fig.

S10). ^{13}C NMR (151 MHz, DMSO-d_6 δ [ppm]): 167.27, 166.98, 163.47, 156.49, 150.60, 150.03, 149.09, 148.67, 146.21, 145.87, 141.42, 140.32, 139.83, 137.90, 137.70, 137.11, 136.55, 131.70, 131.56, 131.41, 130.23, 129.65, 129.61, 129.08, 128.99, 128.08, 126.72, 126.30, 125.54, 125.20, 124.85, 124.35, 123.00, 120.77, 120.54, 113.87, 113.34, 113.15 (Fig. S11). MS:(MALDI-TOF) [m/z]: 1132.37 (M^+) (Fig. S12). Calcd. for $C_{66}H_{49}F_6IrN_7P$: C 62.06, H, 3.87, N 7.68. Found: C 62.05, H 3.87, N 7.66.

Ir4: dark red solid. Yield: 35%. ^{1}H NMR (500 MHz, DMSO-d_6 δ [ppm]): 9.41 (d, J = 7.5 Hz, 1H), 9.17 – 9.15 (m, 2H), 8.81 (d, J = 7.9 Hz, 1H), 8.57 (d, J = 8.0 Hz, 1H), 8.52 (d, J = 8.3 Hz, 1H), 8.48 (d, J = 8.4 Hz, 1H), 8.35 (d, J = 7.9 Hz, 1H), 8.24 (t, J = 9.0 Hz, 2H), 8.17 (t, J = 7.8 Hz, 1H), 8.11 (d, J = 8.0 Hz, 1H), 8.04 – 7.91 (m, 4H), 7.90 (d, J = 5.4 Hz, 1H), 7.85 (t, J = 7.5 Hz, 1H), 7.80 – 7.76 (m, 2H), 7.52 (t, J = 6.4 Hz, 1H), 7.45 (d, J = 7.0 Hz, 1H), 7.16 (t, J = 7.7 Hz, 1H), 7.10 (d, J = 8.8 Hz, 1H), 7.06 (t, J = 7.7 Hz, 1H), 6.72 (d, J = 7.6 Hz, 1H), 6.21 (d, J = 7.6 Hz, 1H), 6.09 (d, J = 8.5 Hz, 2H), 5.77 (d, J = 8.5 Hz, 2H), 5.33 (s, 2H) (Fig. S13). ^{13}C NMR (151 MHz, DMSO-d_6 δ [ppm]): 156.41, 156.01, 150.69, 144.97, 143.91, 142.66, 142.62, 140.89, 140.54, 139.86, 139.38, 135.13, 134.59, 134.52, 133.13, 133.02, 132.71, 132.63, 132.56, 132.42, 132.14, 132.05, 131.53, 131.48, 131.25, 130.73, 130.66, 130.09, 129.62, 129.24, 128.87, 128.82, 126.33, 124.63, 124.54, 124.22, 123.92, 122.93, 112.49 (Fig. S14). MS:(MALDI-TOF) [m/z]: 948.24 (M^+) (Fig. S15). Calcd. for $C_{52}H_{33}F_6IrN_7P$: C 57.14, H, 3.04, N 8.97. Found: C 57.14, H 3.06, N 9.00.

Ir5: reddish brown solid. Yield: 48%. ^{1}H NMR (500 MHz, DMSO-d_6 δ [ppm]): 9.41 (d, J = 8.1 Hz, 1H), 9.28 (s, 1H), 9.21 (d, J = 11.2 Hz, 2H), 9.16 (d, J = 8.0 Hz, 1H), 8.95 (s, 1H), 8.78 (d, J = 7.8 Hz, 1H), 8.52 (d, J = 7.8 Hz, 1H), 8.40 (dd, J = 8.6, 3.6 Hz, 2H), 8.34 (d, J = 7.8 Hz, 1H), 8.22 (t, J = 7.8 Hz, 1H), 8.14 (t, J = 7.4 Hz, 2H), 8.07 (d, J = 8.0 Hz, 1H), 8.01 (s, 1H), 7.94 (d, J = 7.9 Hz, 1H), 7.85 (d, J = 7.1 Hz, 1H), 7.78 (d, J = 7.9 Hz, 1H), 7.70 (dd, J = 11.3, 6.9 Hz, 3H), 7.57 (d, J = 7.5 Hz, 3H),

7.48 (d, *J* = 8.3 Hz, 1H), 7.12 (t, *J* = 7.7 Hz, 1H), 7.05 (d, *J* = 8.5 Hz, 1H), 7.01 (t, *J* = 7.7 Hz, 1H), 6.86 (d, *J* = 7.6 Hz, 1H), 6.33 (d, *J* = 7.7 Hz, 1H), 6.29 (d, *J* = 8.8 Hz, 2H), 5.83 (d, *J* = 8.8 Hz, 2H), 5.40 (s, 2H) (Fig. S16). ^{13}C NMR (151 MHz, DMSO-d_6 δ [ppm]): 162.78, 154.49, 154.31, 152.93, 150.24, 144.61, 144.32, 142.77, 142.65, 141.96, 141.67, 140.79, 139.66, 138.15, 137.46, 135.93, 135.31, 134.69, 134.23, 133.62, 133.30, 132.81, 132.59, 132.37, 131.20, 130.47, 130.31, 130.18, 129.85, 129.40, 129.17, 128.90, 128.82, 127.85, 126.40, 126.16, 126.10, 124.56, 124.29, 124.18, 124.00, 122.15, 112.73 (Fig. S17). MS:(MALDI-TOF) [m/z]: 1048.27 (M^+) (Fig. S18). Calcd. for $C_{60}H_{37}F_6IrN_7P$: C 60.40, H, 3.13, N 8.22. Found: C 60.38, H 3.12, N 8.22.

Preparation of Ir5 NPs

Ir5 (2 mg) and mPEG-SC-2000 (PEG-NHS-2000) (4 mg) were mixed (1:1 wt/wt), and dissolved in DMSO (2 mL) with stirring overnight in room temperature. Subsequently, the product was dialyzed in water (3500 kD) to obtain water-soluble nanoparticles that passed through a 0.22 μm filter membrane to obtain **Ir5 NPs**. **Ir5** is a hydrophobic material and PEG is a hydrophilic polymer, after dialyzed in water, the hydrophobic **Ir5** molecules are located within the nanoparticles, while the hydrophilic PEG is deployed on the outer side, as shown in the nanoparticles in Scheme 1, and the NPs can be dispersed in water. The content of **Ir5** in **Ir5 NPs** was calculated using the standard curve (Fig. S19) to be 42% wt.

UV–vis absorption spectra and emission spectra

*UV–vis absorption spectra***:**

10 μM **Ir1-Ir5** in the mixed solvent (CH_3CN:H_2O =1:90 v/v) were tested.

The concentration of **Ir5 NPs** in H_2O was calculated to contain 10 μM **Ir5**.

*Emission spectra***:**

10 μM **Ir1-Ir5** in the mixed solvent (CH_3CN:H_2O =1:90 v/v) were tested with λ_{ex} = 450 nm. The concentration of **Ir5 NPs** in H_2O was calculated to contain 10 μM **Ir5**. λ_{ex} =655 nm.

ROS Generation in Solution

Detection method for total ROS

DCFH detection of total ROS: ROS enhance the fluorescence emission of DCFH at 525 nm, and the ROS production can be evaluated by emission spectral changes. PSs and 5 μM DCFH were mixed thoroughly in a quartz colorimetric dish and emission spectra were detected under different conditions. PSs concentration: **Ir1-Ir5**: 10 μM; **Ir5 NPs**: 10 μg/mL. Light source: White LED (400-800 nm) 20 mW cm^{-2} for **Ir1-Ir5**; 655 nm laser 150 mW cm^{-2} for **Ir5 NPs**. I_0 = initial intensity at 525 nm. I = real-time intensity at 525 nm with various times of light exposure.

Detection method for $^1O_2$

ABDA detection of $^1O_2$: $^1O_2$ will oxidize ABDA and cause its degradation, resulting in a decrease in absorption at 378 nm. The material's ability to produce $^1O_2$ can be evaluated by its change in absorption intensity. PSs and 25 μg/mL ABDA were mixed thoroughly in a quartz cuvette and absorption spectra were obtained under different conditions. PSs concentration: **Ir1-5**: 10 μM; **Ir5 NPs**: 10 μg/mL. Light source: White LED (400-800 nm) 20 mW cm^{-2} for **Ir1-Ir5**; 655 nm laser 150 mW cm^{-2} for **Ir5 NPs**. A_0 = initial absorbance of 378 nm. A = real-time absorbance of 378 nm with various light exposure times.

TEMP detection of $^1O_2$: $^1O_2$ can oxidize TEMP, forming TEMPO radicals which are then detected by electron paramagnetic resonance spectroscopy. 10 μL TEMP was added to 10 μM **Ir1**-**Ir5**, the solution was irradiated with white LED (400-800 nm) at 20 mW cm^{-2} for 5 min before monitoring. Microwave power 5.012 mW.

Detection method for $O_2^{\bullet-}$

DHR-123 detection of $O_2^{\bullet-}$: $O_2^{\bullet-}$enhances the fluorescence emission of DHR-123 at 525 nm through an oxidation reaction. The $O_2^{\bullet-}$ production ability of the material can be evaluated by changes in its emission spectrum. PSs and 5 μM DHR-123 were mixed thoroughly in a quartz colorimetric dish and absorption spectra were obtained under different conditions. PSs concentration: **Ir1**-**Ir5**: 10 μM; **Ir5 NPs**: 10 μg/mL. Light source: White LED (400-800 nm) 20 mW cm^{-2} for **Ir1**-**Ir5**; 655 nm laser 150 mW cm^{-2} for **Ir5 NPs**. I_0 = initial intensity of 525 nm. I = real-time intensity of 525 nm with various times of light exposure.

DMPO detection of $O_2^{\bullet-}$: DMPO can be used as an $O_2^{\bullet-}$ capture agent to form addition products, which are detected by electron paramagnetic resonance spectroscopy. 20 mM DMPO methanol solution (30 μL) was added to 10 μM **Ir1**-**Ir5**, the solution was irradiated with a white LED (400-800 nm) at 20 mW cm^{-2} for 5 min before monitoring the spectrum. Microwave power 5.012 mW.

Detection method for •OH

HPF detection of •OH: •OH enhances the fluorescence emission of HPF at 515 nm through an oxidation reaction. The •OH production ability of the material can be evaluated by changes in its emission spectrum. PSs and 3 μM HPF were mixed thoroughly in a quartz colorimetric dish, detect absorption spectra under different conditions. PSs concentration: **Ir1**-**Ir5**: 10 μM; **Ir5 NPs**: 10 μg/mL. Light source: White LED (400-800 nm) 20 mW cm^{-2} for **Ir1**-**Ir5**; 655 nm laser 150 mW cm^{-2} for **Ir5 NPs**. I_0 = initial intensity of 515 nm. I = real-time intensity of 515 nm with various times of light exposure.

Cell Culture

4T1 cells were cultured in this experiment. The culture medium was prepared by RPMI Medium 1640 containing 10% (v:v) FBS. The cell culture flask was placed in an incubator at: (a) Normoxic conditions: Cells were maintained in a humidified atmosphere containing 5% CO_2 of 37 °C; (b) Hypoxic conditions: Cells was maintained at 37 °C in a humidified atmosphere containing 1% O_2, 5% CO_2, 94% N_2.

Cytotoxicity test method

The cytotoxicity of **Ir5 NPs** was detected by MTT assay. 4T1 cells were seeded in 96-well plates at a density of 10,000 cells per well and cultured in an incubator at different conditions (normoxia or hypoxia) for 24 h. After aspirating the old culture medium, 100 μL RPMI Medium 1640 containing different concentration of **Ir5 NPs** (0-32 μg mL^{-1}) were added to each well. The original culture mediums were replaced by 100 μL fresh RPMI Medium 1640 after 6 h and irradiated with 655 nm laser, 150 mW cm^{-2} for 8 min. After irradiation, the cells were placed in the incubator for 24 h. Then, the cells' viability was detected by MTT assay. The cytotoxicity of RB, Ce6, ZnPc and HpD were detected using the same method.

Intracellular uptake and localization measurements

4T1 cells were seeded in confocal culture dishes at a density of 50,000 cells per well. RPMI Medium 1640 containing **Ir5 NPs** (10 μg mL^{-1}) was incubated for 1 h, 3 h and 6 h, respectively. After incubation, the cells were then stained with DAPI and MitoTracker Green. The cells were then washed twice with PBS, and fresh medium was replenished before visualization by CLSM. The co-staining with DAPI and MitoTracker Green enables the simultaneous determination of cellular uptake and co-localization abilities.[6]

Evaluation of intracellular ROS production capacity

4T1 cells were seeded in confocal dishes at a density of 50,000 cells per well. Different formulations (Control, **Ir5 NPs**+Laser, **Ir5 NPs**+Dark) were added to the medium and the cells were incubated for another 24 h. For ROS level tests, DCFH-DA (1 μL) [or SOSG (1 μL), or DHR-123 (3 μL)] was added to the confocal culture dish. After treatment in the dark for 20 min, the medium containing the indicator was aspirated, washed twice with PBS, and imaged by CLSM. The green fluorescence intensity of the indicators in the cells was observed: λ_{ex}= 465-495 nm, λ_{em}= 515-555 nm.

Live/Dead Staining Test Methods

4T1 cells were seeded in confocal dishes at a density of 50,000 cells per well. Different formulations (Control, **Ir5 NPs**+Laser, **Ir5 NPs**+Dark) were added to the medium and the cells were incubated for another 24 h. Detection buffer containing Calcein-AM and PI was added to the confocal dishes. The fluorescence images were observed under an inverted fluorescence microscope to determine the cell survival state. λ_{ex}= 540-580 nm, λ_{em}= 600-660 nm for PI and λ_{ex}= 465-495 nm, λ_{em}= 515-555 nm for Calcein-AM.

Detection of Mitochondrial Membrane Potential.

The 4T1 cells were incubated in a glass-bottom dish at a density of 50,000 cells per dish for 24 h, and then the cells were subjected to different treatments (Control, **Ir5 NPs**+Laser, **Ir5 NPs**+Dark). After 24 h, the culture medium was replaced. Next, the cells were incubated with JC-1 (5 μg/mL) at 37 °C for 20 min. Then, the cells were washed three times with PBS. After that, the cells were imaged by CLSM. λ_{ex}= 540-580 nm, λ_{em}= 600-660 nm for J-A and λ_{ex}= 465-495 nm, λ_{em}= 515-555 nm for J-M (A = aggregated; M = monomeric).

Annexin V-FTIC/PI assays

4T1 cells were seeded in confocal dishes at a density of 50,000 cells per well. Different formulations (Control, **Ir5 NPs**+Laser, **Ir5 NPs**+Dark) were added to the medium and the cells were incubated for another 24 h. Finally, the cells were stained with Annexin-FITC/PI for 15 min and then were imaged by CLSM. λ_{ex}= 540-580 nm, λ_{em}= 600-660 nm for PI and λ_{ex}= 465-495 nm, λ_{em}= 515-555 nm for Annexin V-FTIC.

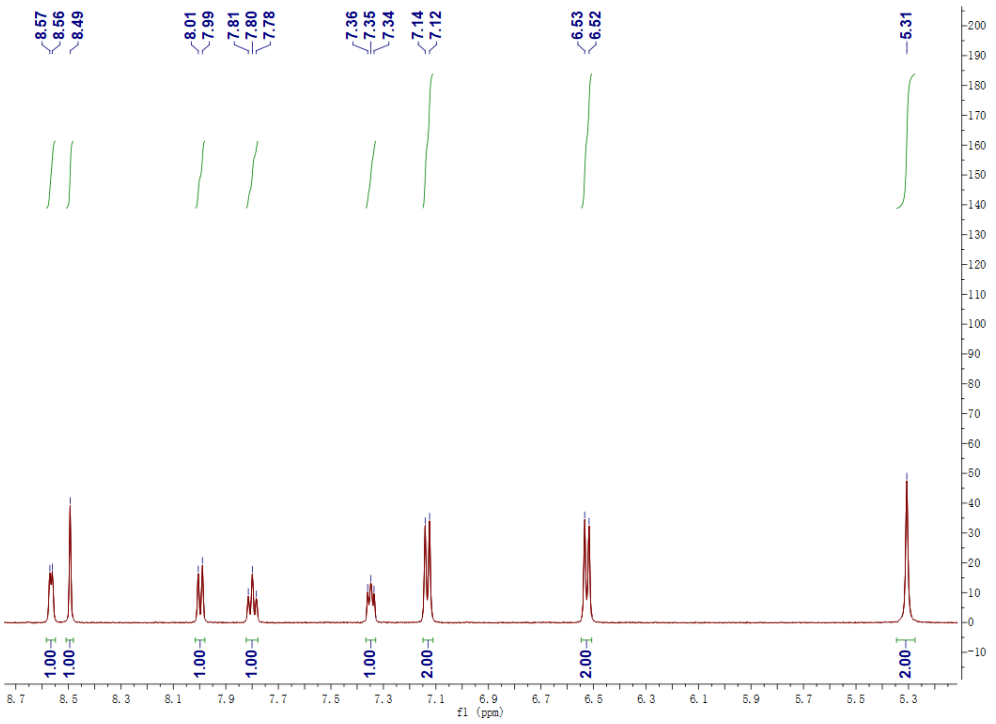

Fig. S1 ^{1}H NMR spectrum of **Schiff-NH$_2$** in DMSO-*d$_6$* at room temperature.

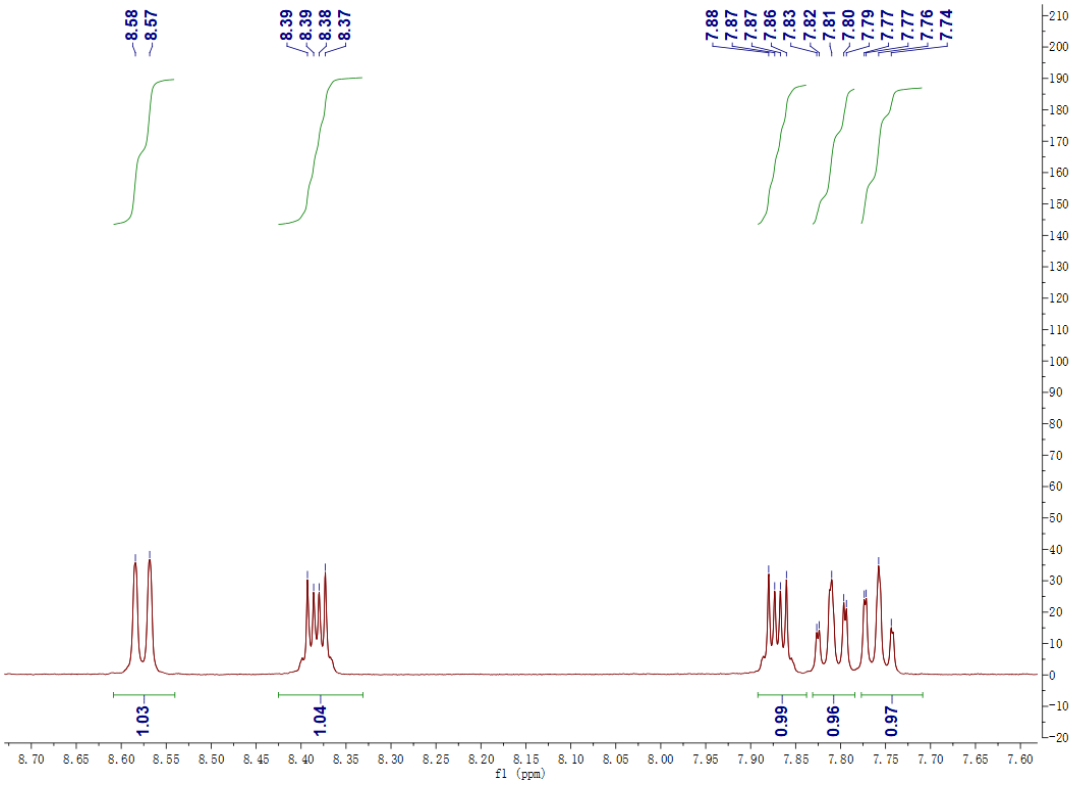

Fig. S2 ^{1}H NMR spectrum of **L4** in $CDCl_3$ at room temperature.

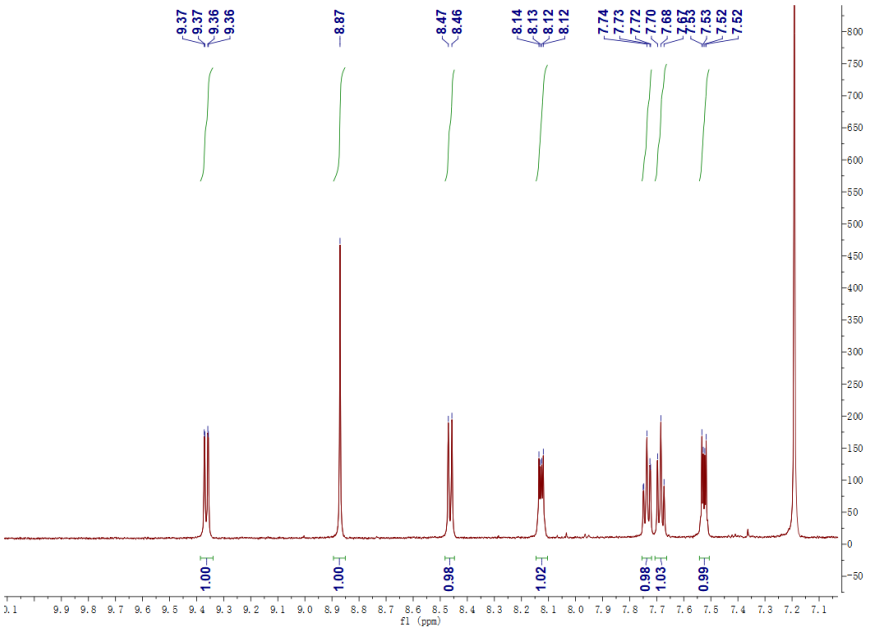

Fig. S3 ^{1}H NMR spectrum of **L5** in $CDCl_3$ at room temperature.

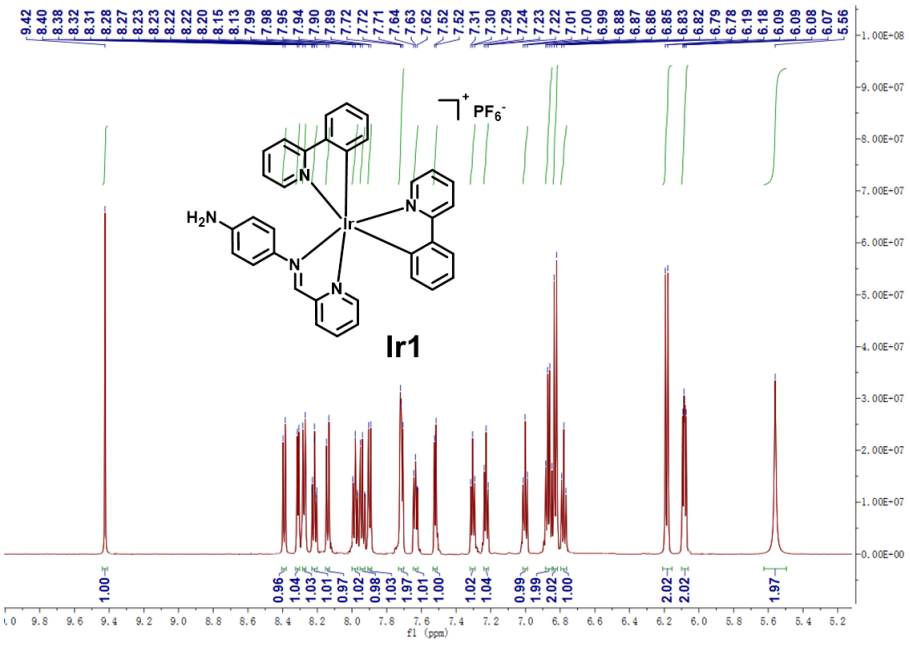

Fig. S4 ^{1}H NMR spectrum of **Ir1** in DMSO-d_6 at room temperature.

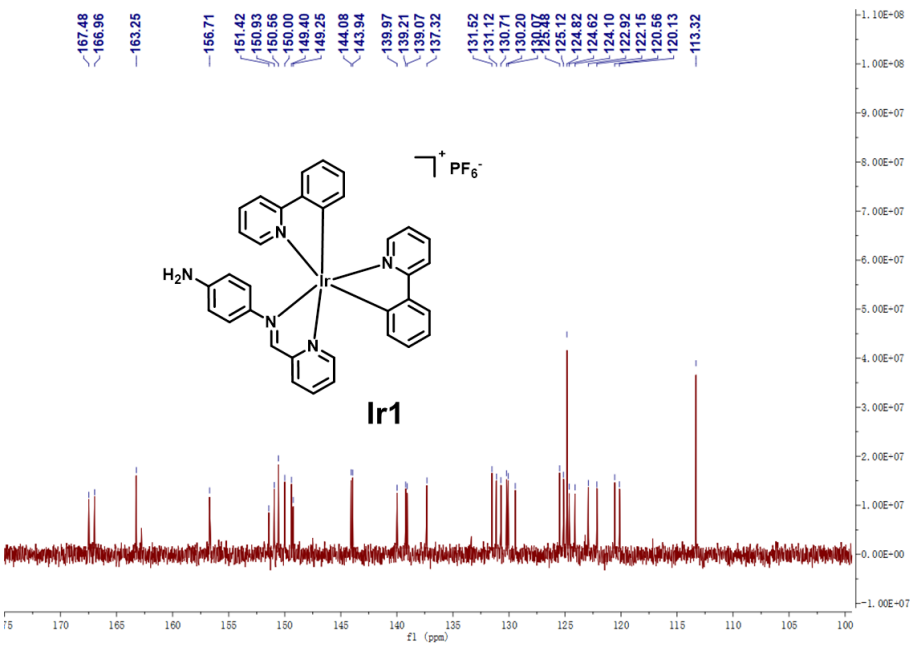

Fig. S5 ^{13}C NMR spectrum of **Ir1** in DMSO-d_6 at room temperature.

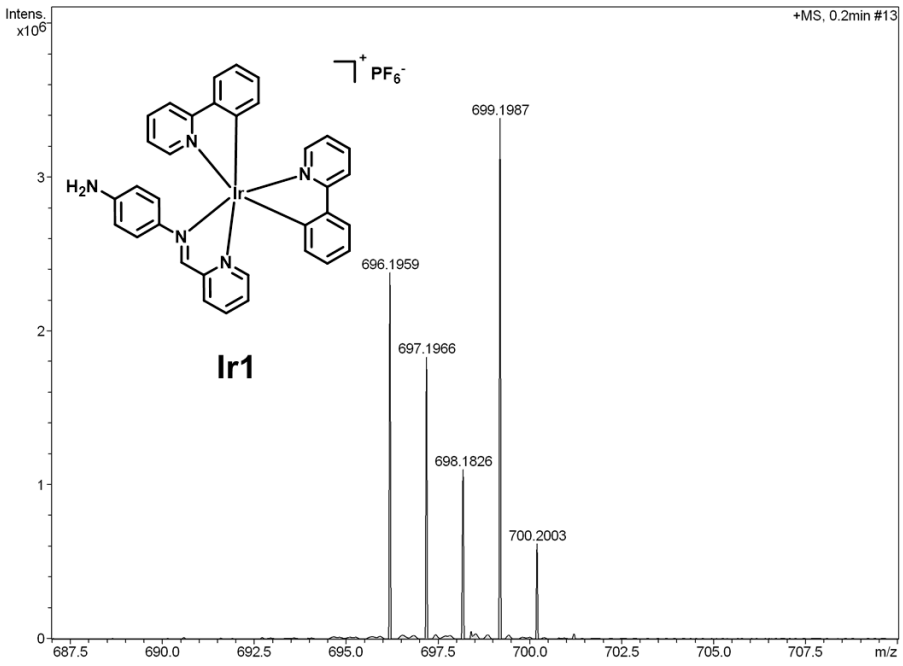

Fig. S6 Mass spectrum of **Ir1** at room temperature.

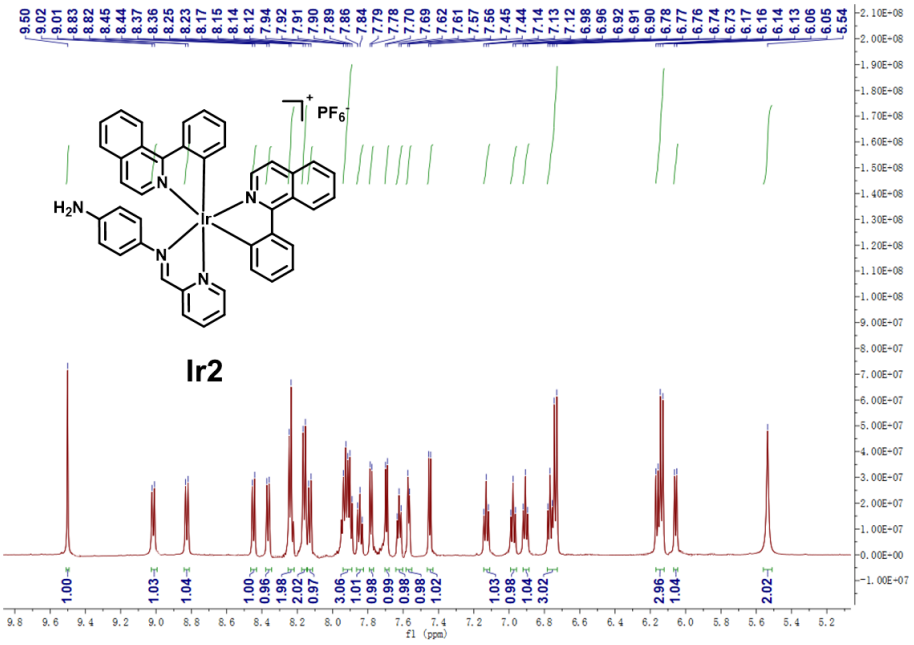

Fig. S7 ^{1}H NMR spectrum of **Ir2** in DMSO-d_6 at room temperature.

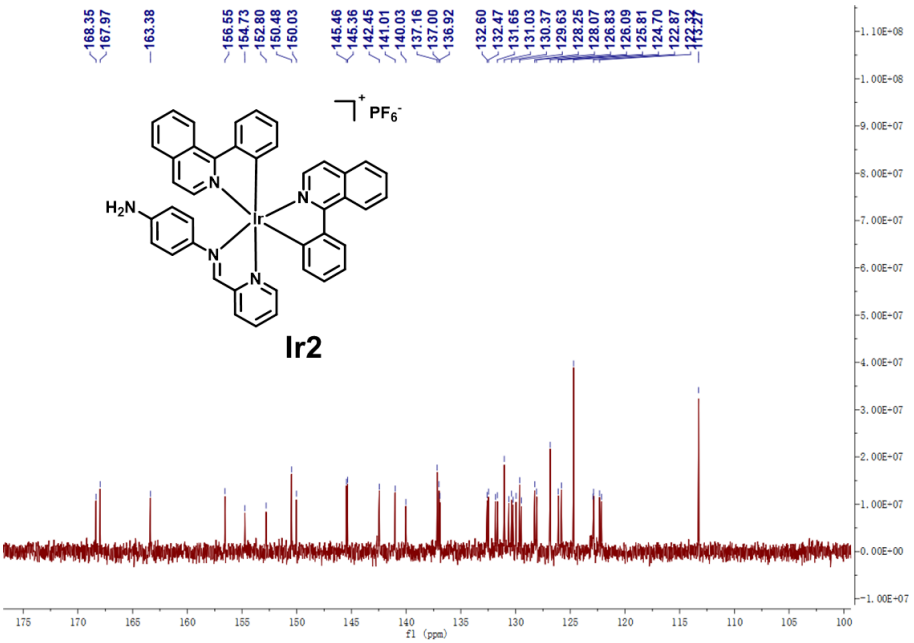

Fig. S8 ^{13}C NMR spectrum of **Ir2** in DMSO-d_6 at room temperature.

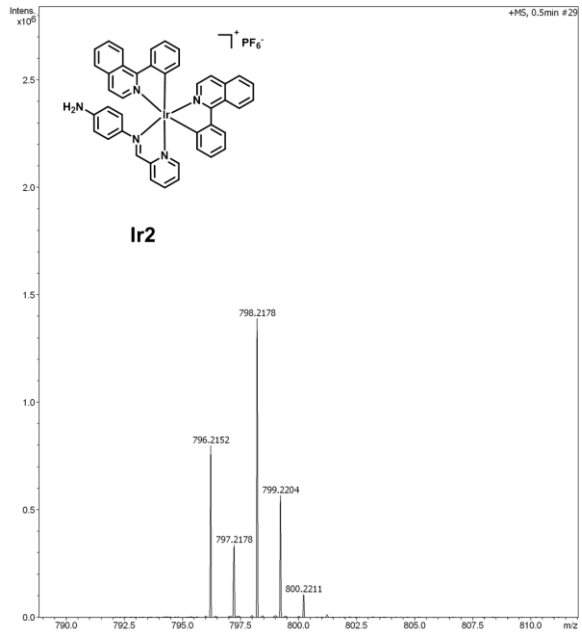

Fig. S9 Mass spectrum of **Ir2** at room temperature.

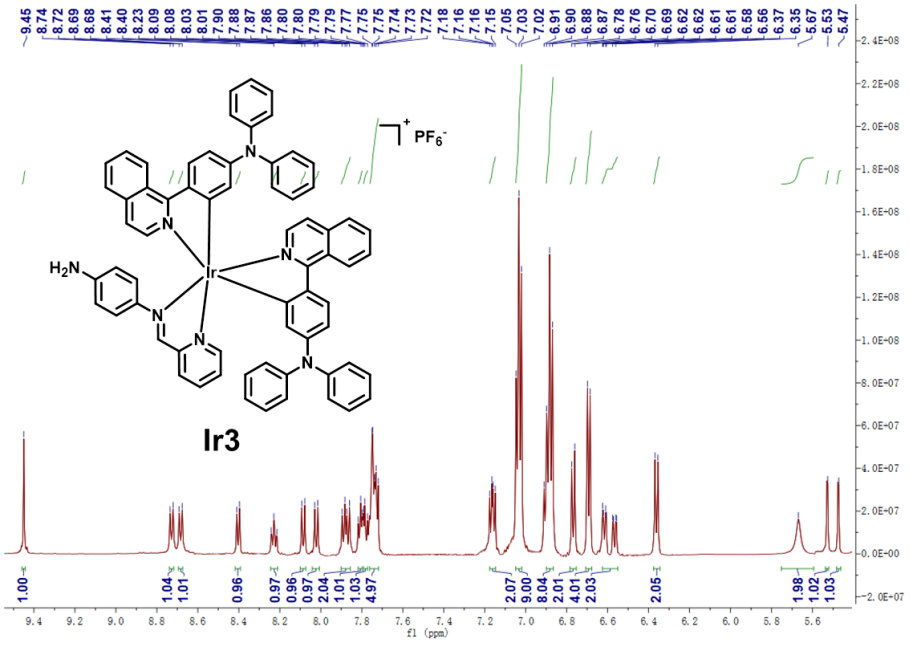

Fig. S10 ^{1}H NMR spectrum of **Ir3** in DMSO-d_6 at room temperature.

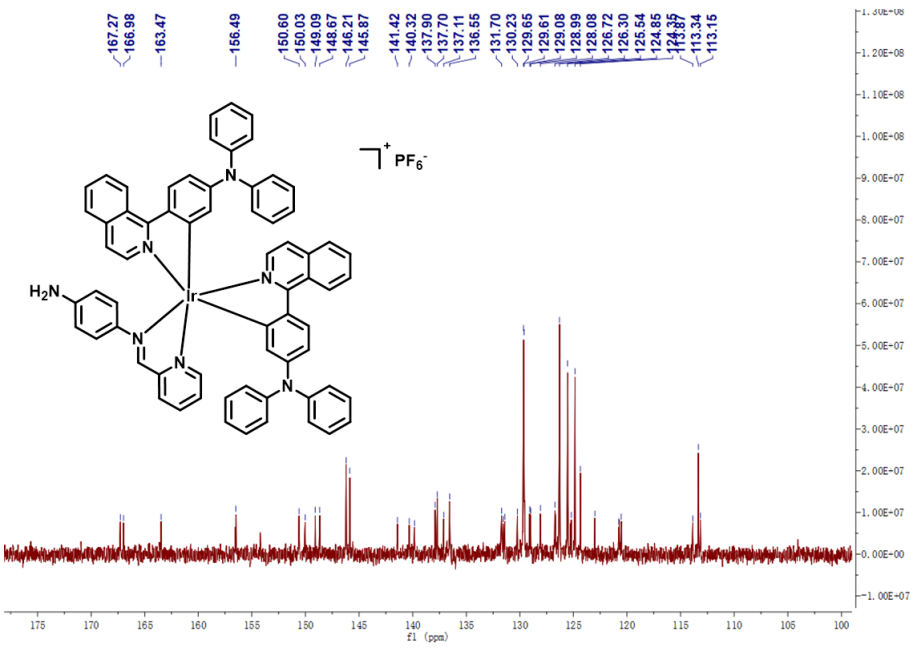

Fig. S11 ^{13}C NMR spectrum of **Ir3** in DMSO-d_6 at room temperature.

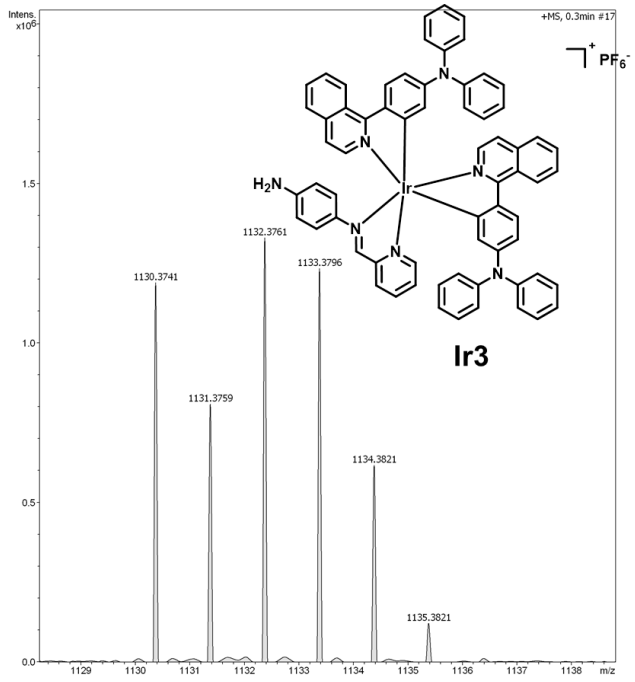

Fig. S12 Mass spectrum of **Ir3** at room temperature.

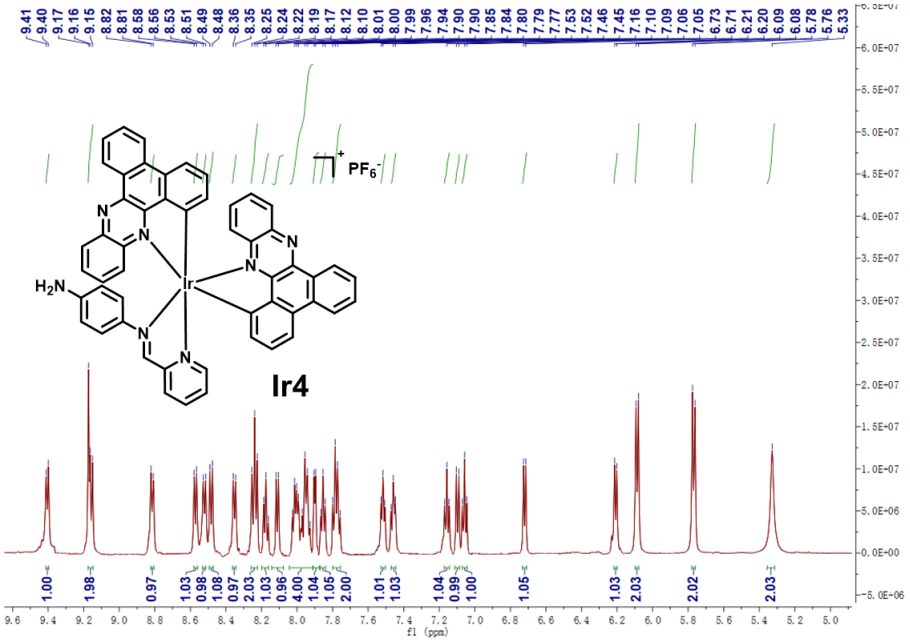

Fig. S13 ^{1}H NMR spectrum of **Ir4** in DMSO-d_6 at room temperature.

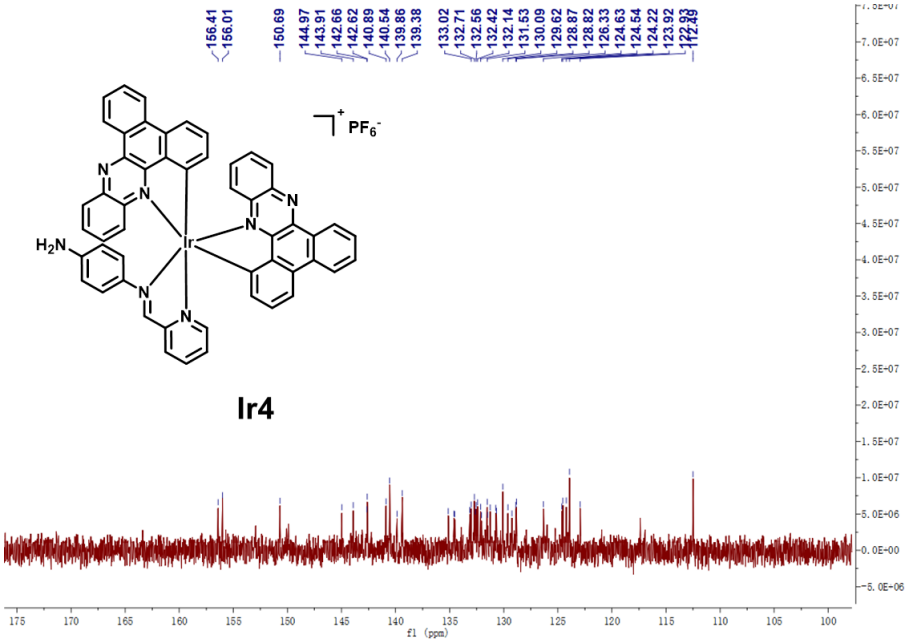

Fig. S14 ^{13}C NMR spectrum of **Ir4** in DMSO-d_6 at room temperature.

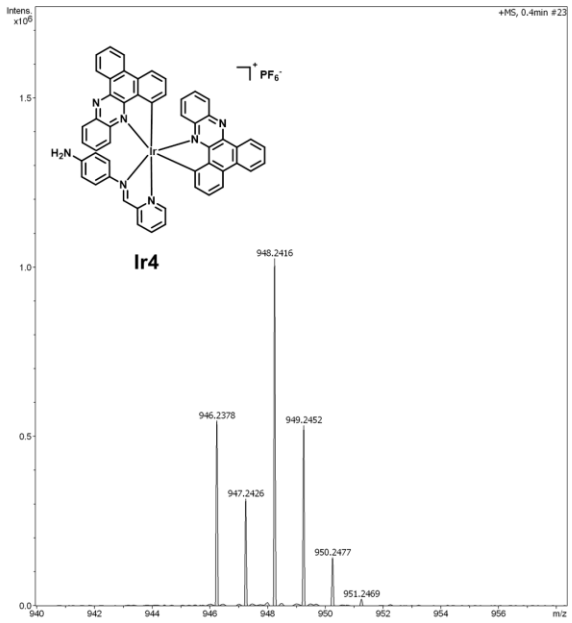

Fig. S15 Mass spectrum of **Ir4** at room temperature.

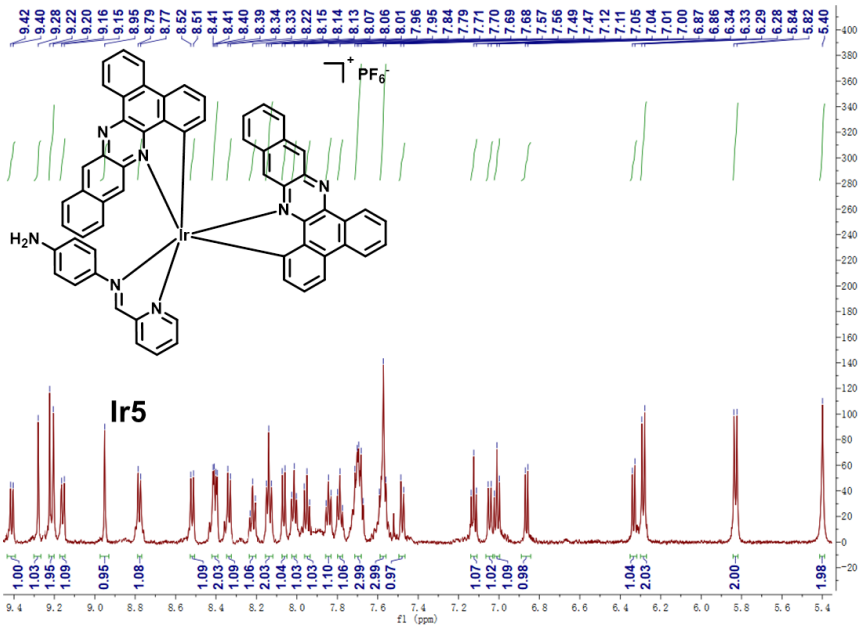

Fig. S16 ^{1}H NMR spectrum of **Ir5** in DMSO-d_6 at room temperature.

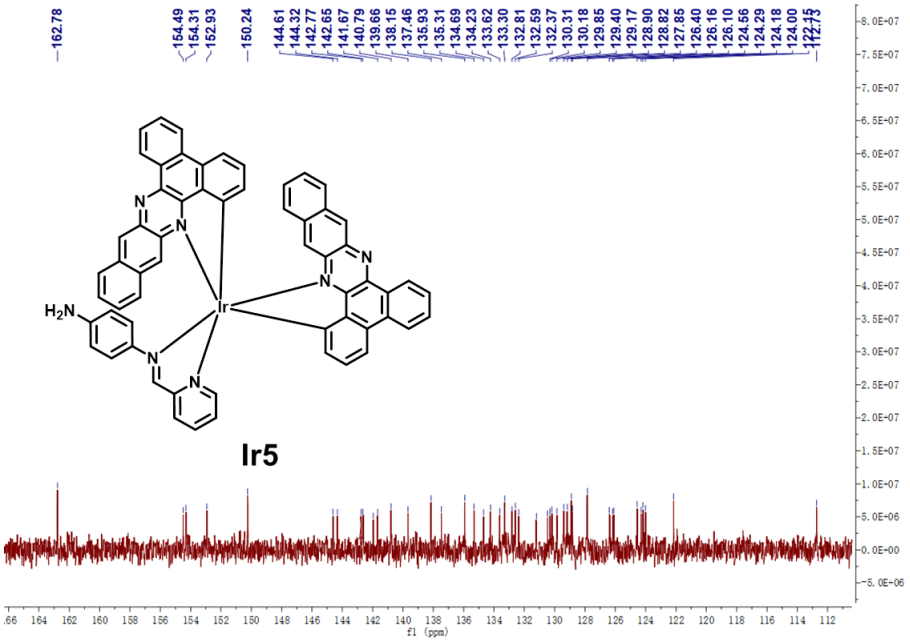

Fig. S17 ^{13}C NMR spectrum of **Ir5** in DMSO-d_6 at room temperature.

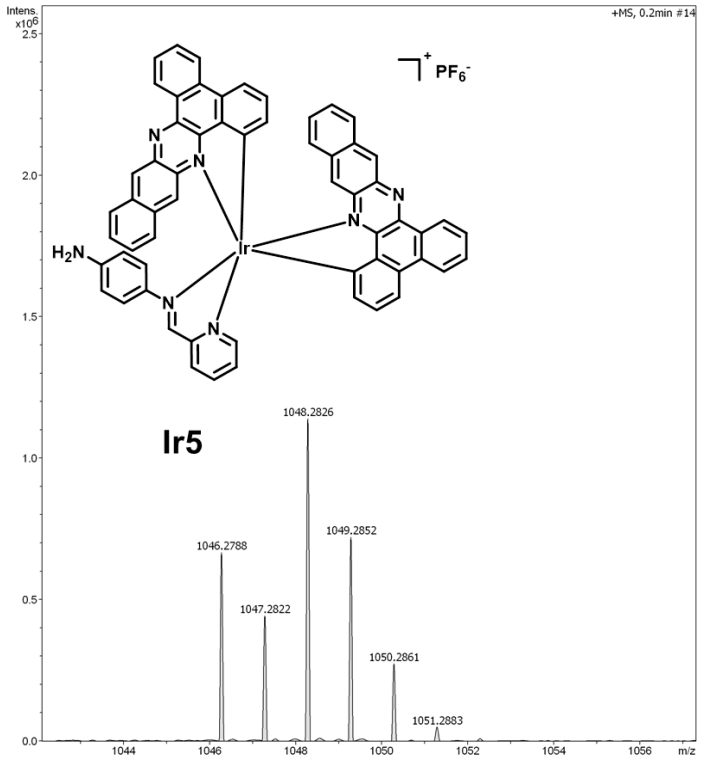

Fig. S18 Mass spectrum of **Ir5** at room temperature.

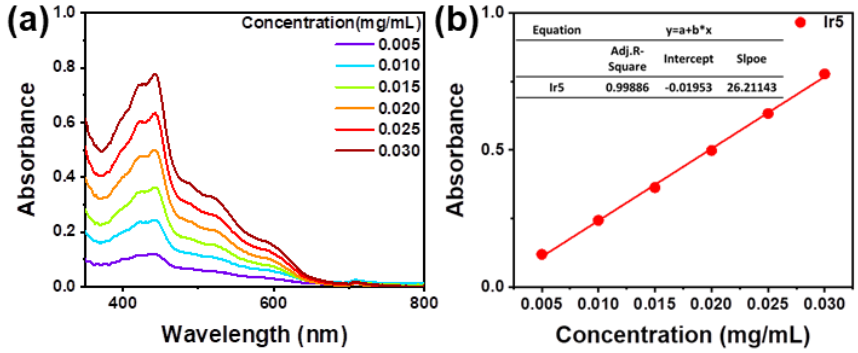

Fig. S19 (a) UV–vis absorption spectra of **Ir5** in CH_3CN:H_2O (1:90 v/v). (b) Standard curve of **Ir5**.

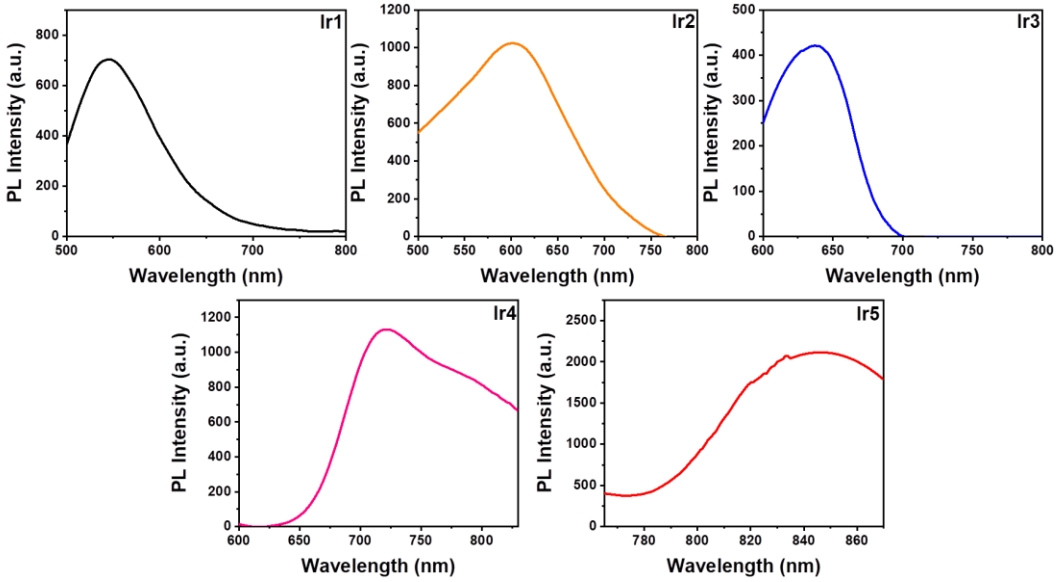

Fig. S20 Emission spectra of **Ir1-Ir5** in CH_3CN:H_2O (1:90 v/v).

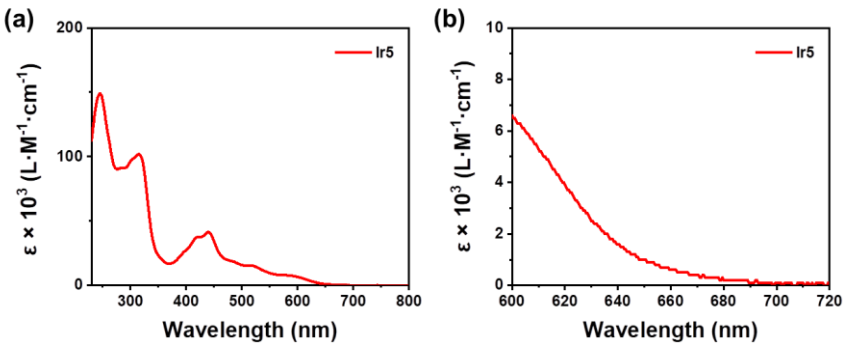

Fig. S21 (a) The molar absorptivity spectrum of **Ir5**. (b) The enlarged molar absorptivity spectrum (from 600 nm to 720 nm).

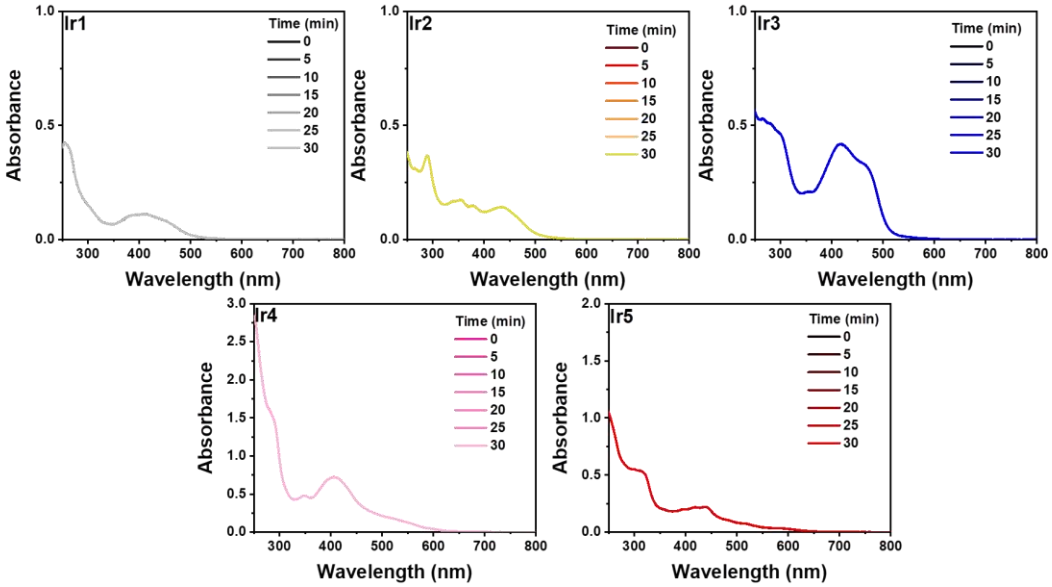

Fig. S22 UV–vis absorption spectra of **Ir1-Ir5** upon exposure to white LED (400-800 nm) at 20 mW cm^{-2} in 30 min.

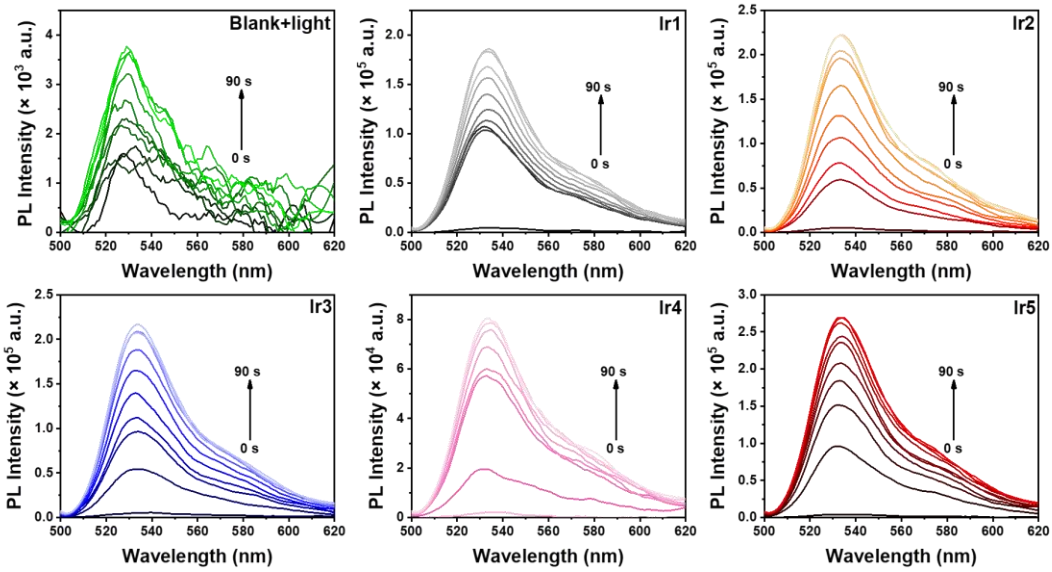

Fig. S23 Total ROS generation of **Ir1-Ir5** upon exposure to white LED (400-800 nm) at 20 mW cm^{-2}. Indicator: DCFH.

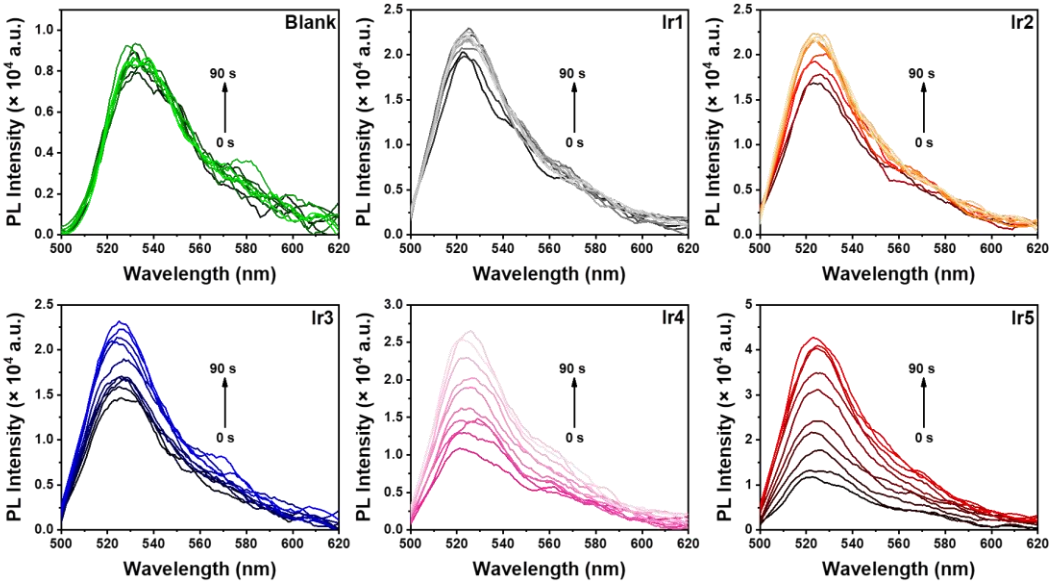

Fig. S24 $O_2^{\bullet-}$ generation of **Ir1-Ir5** upon exposure to white LED (400-800 nm) at 20 mW cm^{-2}. Indicator: DHR-123.

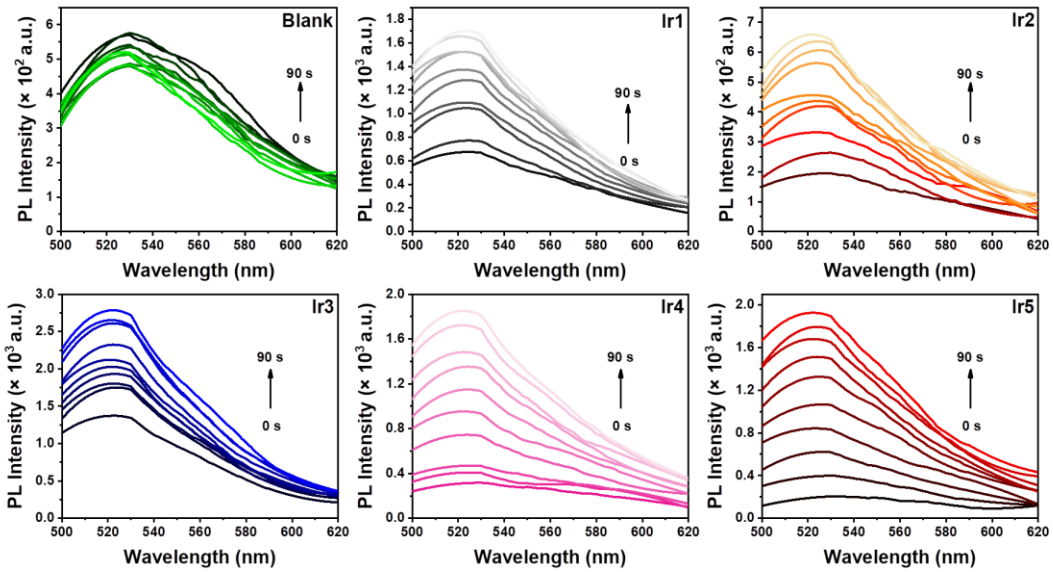

Fig. S25 •OH generation of **Ir1-Ir5** upon exposure to white LED (400-800 nm) at 20 mW cm^{-2}. Indicator: HPF.

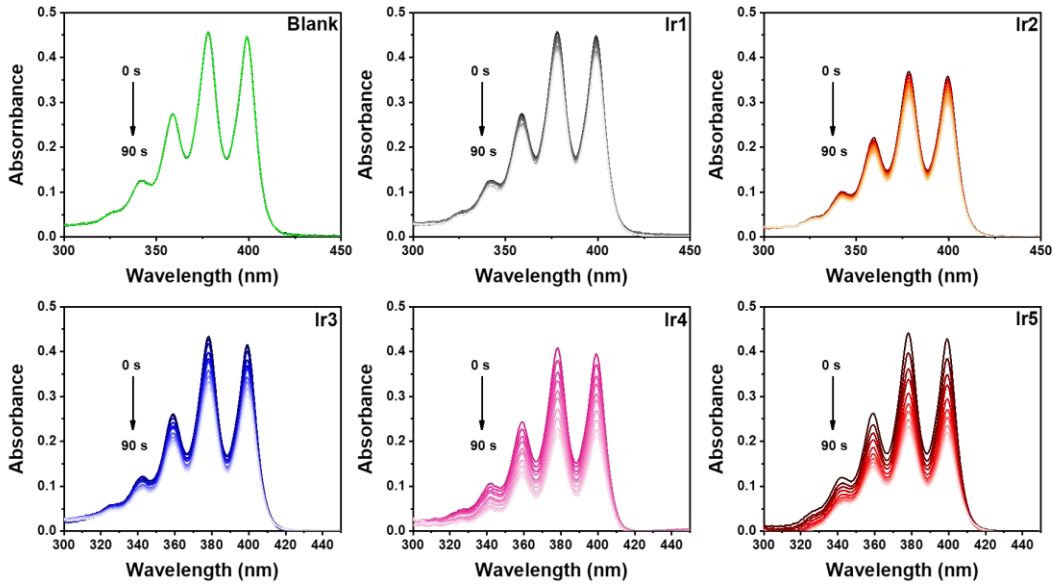

Fig. S26 $^1O_2$ generation of **Ir1-Ir5** upon exposure to white LED (400-800 nm) at 20 mW cm^{-2}. Indicator: ABDA.

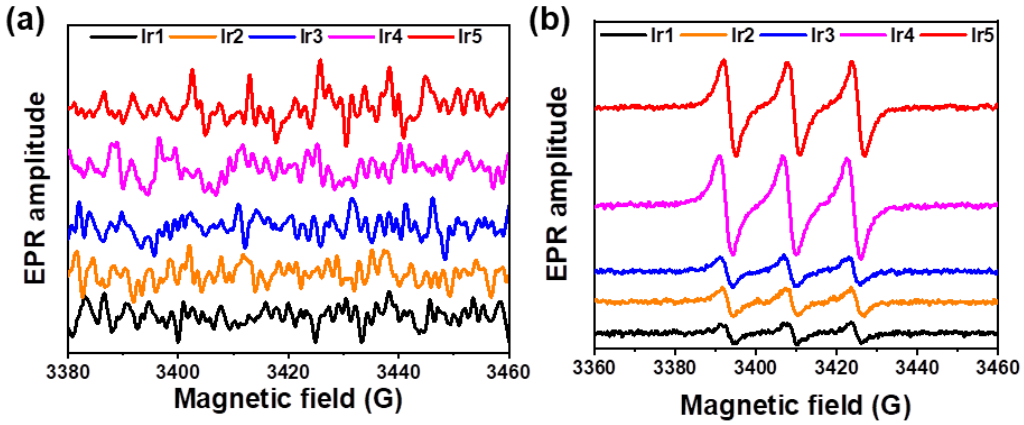

Fig. S27 EPR detection of **Ir1-Ir5**. (a) $O_2^{\bullet-}$ generation of **Ir1- Ir5** upon exposure to white LED (400-800 nm) at 20 mW cm^{-2}. Indicator: DMPO. (b) $^1O_2$ generation of **Ir1-Ir5** upon exposure to white LED (400-800 nm) at 20 mW cm^{-2}. Indicator: TEMP.

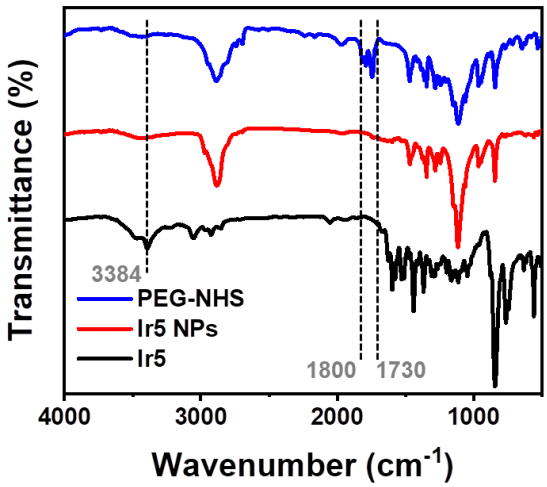

Fig. S28 FT-IR spectra of PEG-NHS (PEG-Sc), **Ir5 NPs** and **Ir5**.

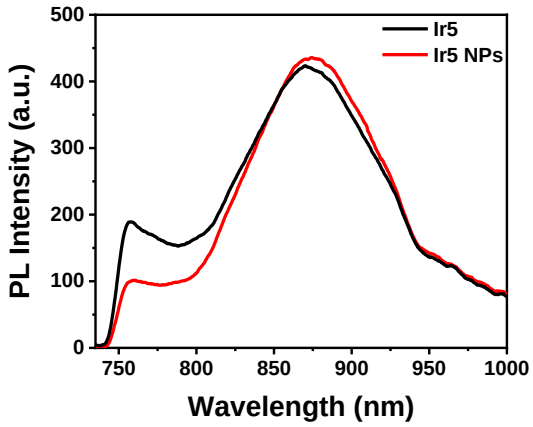

Fig. S29 Emission spectra of **Ir5 NPs** and **Ir5**.

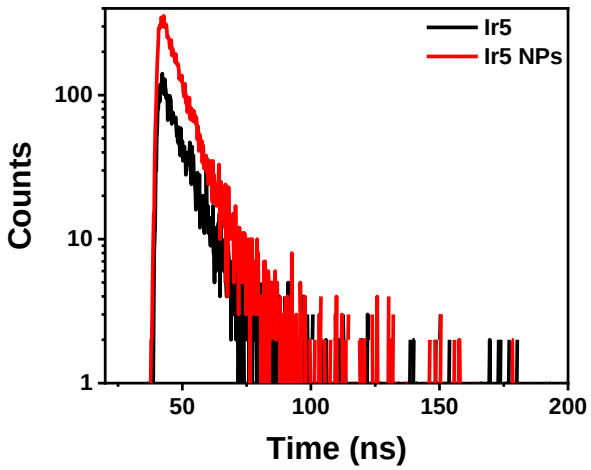

Fig. S30 Luminescence decay curves of **Ir5 NPs** and **Ir5**. The construction of **Ir5 NPs** increases the excited state lifetime of **Ir5**, which is positive for PDT processes.

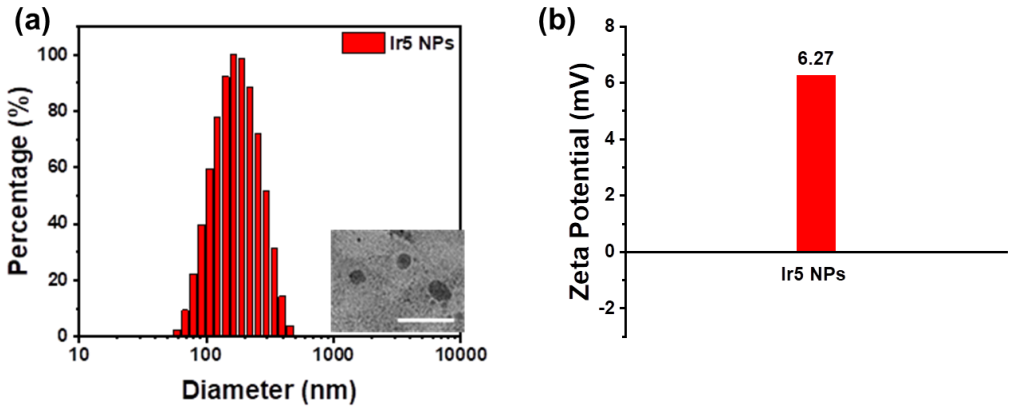

Fig. S31 (a) DLS data for **Ir5 NPs**. Inset: TEM image of **Ir5 NPs**. Scale bar = 500 nm. (b) The Zeta potential of **Ir5 NPs**.

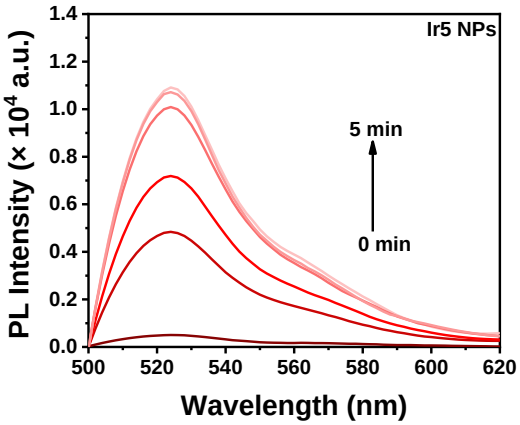

Fig. S32 Total ROS generation of **Ir5 NPs** upon exposure to laser (655 nm) at 150 mW cm^{-2}. Indicator: DCFH.

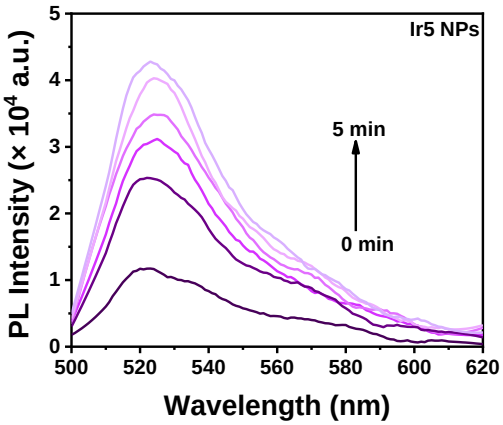

Fig. S33 $O_2^{\bullet-}$ generation of **Ir5 NPs** upon exposure to laser (655 nm) at 150 mW cm^{-2}. Indicator: DHR-123.

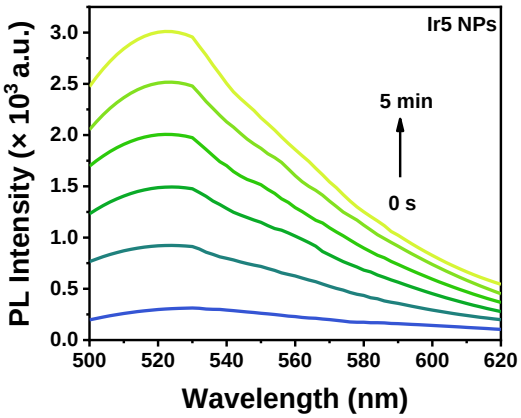

Fig. S34 •OH generation of **Ir5 NPs** upon exposure to laser (655 nm) at 150 mW cm^{-2}. Indicator: HPF.

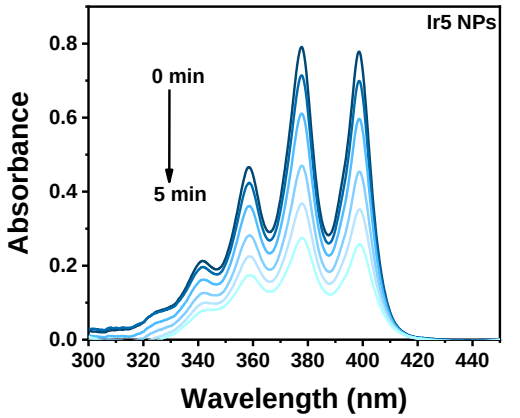

Fig. S35 $^1O_2$ generation of **Ir5 NPs** upon exposure to laser (655 nm) at 150 mW cm^{-2}. Indicator: ABDA.

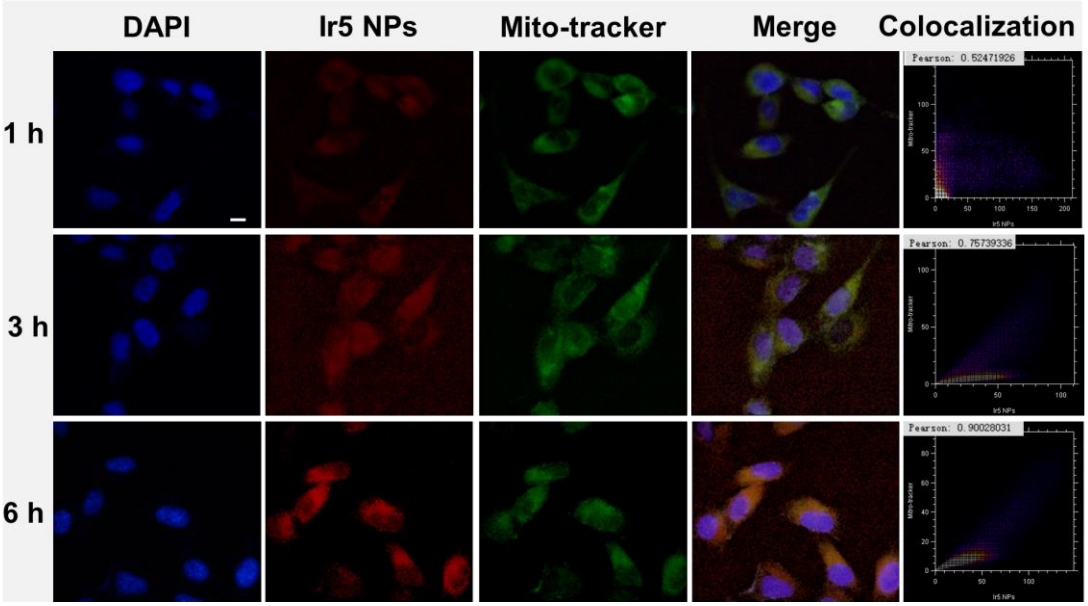

Fig. S36 CLSM images of 4T1 cells after incubation with **Ir5 NPs** and colocalization assay of **Ir5 NPs** with MitoTracker Green. Scale bar = 10 μm.

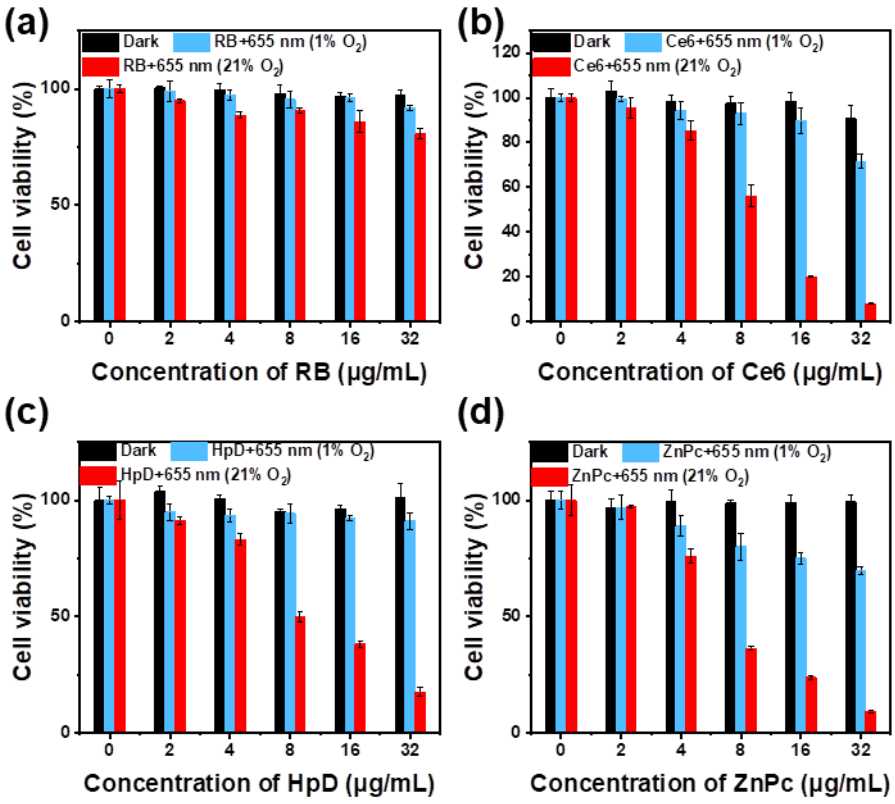

Fig. S37 Relative viability of 4T1 cells after co-incubation with different PSs under different conditions.

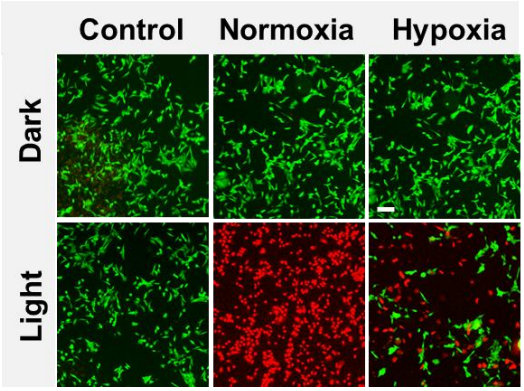

Fig. S38 Confocal fluorescence images of 4T1 cells co-stained with calcein-AM (live cells, green fluorescence) and PI (dead cells, red fluorescence) after treatment **Ir5 NPs** in normoxic and hypoxic conditions. Scale bar = 100 μm.

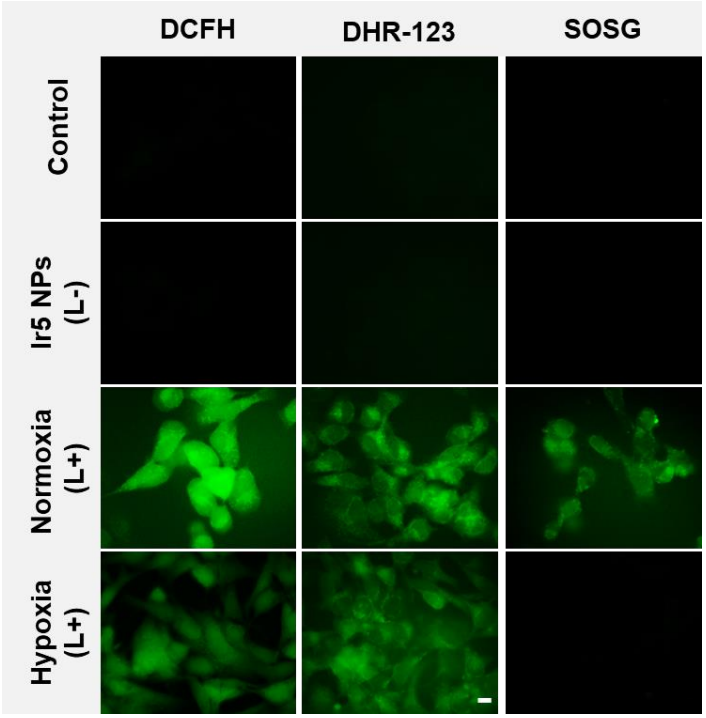

Fig. S39 Confocal fluorescence images for the detection of different types of ROS after being treated with **Ir5 NPs**. (L- is dark group; L+ is after irradiation). Scale bar = 10 μm.

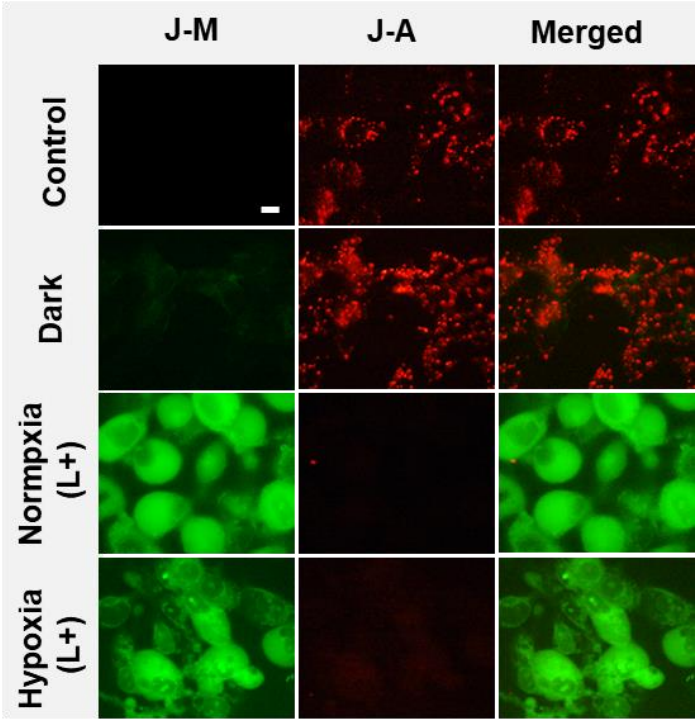

Fig. S40 Confocal fluorescence imaging of MMP in 4T1 cells incubated with **Ir5 NPs** via subsequent JC-1 dye assay. Scale bar = 10 μm.

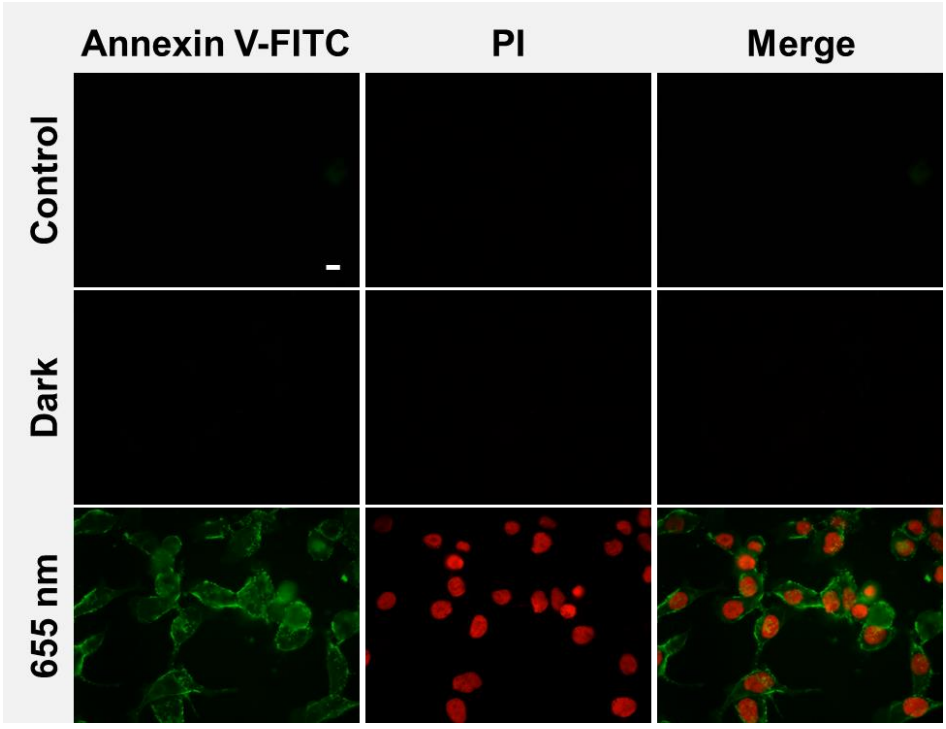

Fig. S41 Death of 4T1 cells induced by **Ir5 NPs** and staining with dual fluorescence of Annexin V-FITC/PI. Scale bar = 10 μm.

Table S1. Photophysical data of **Ir1-Ir5**

	λ_{abs} (nm)	λ_{em} (nm)	Φ_p[c] (%)	τ_p[e] (ns)
Ir1 [a]	257, 405	560 [c]	11.08	7.54
Ir2 [a]	290, 435	600 [c]	2.13	9.38
Ir3 [a]	300, 410, 470	640 [c]	2.34	7.26
Ir4 [a]	290, 405, 530	720 [c]	1.43	8.63
Ir5 [a]	315, 440, 590	845 [c], 875 [d]	1.02	8.35
Ir5 NPs [b]	325, 480, 600	875 [d]	1.04	13.6

[a] Measured in the mixed solvent (CH_3CN:H_2O = 1:90 v/v) (complex concentration = 1.0×10^{-5} M) at room temperature. [b] Measured in H_2O (1.0×10^{-5} M **Ir5** in the **NPs**). [c] λ_{ex} = 450 nm. [d] λ_{ex} = 655 nm. [e] under N_2 conditions. λ_{ex} = 370 nm. According to the literature,[6-10] the short lifetimes of the Ir complexes may be due to nonradiative deactivation processes [involving the electron-donating behavior from the pendent amine and the intramolecular charge transfer (ICT) effect].

Table S2. Cytotoxicity (IC_{50}, μg/mL) of tested materials against 4T1 cell line for 48 h in the absence (dark) and presence of 655 nm (150 mW/cm^2, 8 min) irradiation at normoxic and hypoxic conditions[a]

Materials	Dark	Normoxic		Hypoxic	
		Laser 655 nm	PI[b]	Laser 655 nm	PI[b]
RB	>100	>100	1	>100	1
Ce6	>100	8.64	11.57	>100	1
ZnPc	>100	7.58	13.19	>100	1
HpD	>100	9.64	10.37	>100	1
Ir5 NPs	>100	6.43	15.55	11.71	8.54

[a] Data are presented as the means ± standard deviations (SD) of three repeated measurements.

[b] Phototoxicity index (PI) is defined as the ratio of $^{dark}IC_{50}/^{laser\ (655\ nm)}IC_{50}$

References

1 P. Garra, A. Kermagoret, A. Al Mousawi, F. Dumur, D. Gigmes, F. Morlet-Savary, C. Dietlin, J. P. Fouassier and J. Lalevée, *Polym. Chem.*, 2017, **8**, 4088-4097.

2 S. Liu, J. Han, Y. Chang, W. Wang, R. Wang, Z. Wang, G. Li, D. Zhu and M. R. Bryce, *Chem. Commun.*, 2022, **58**, 10056-10059.

3 S. Liu, J. Han, W. Wang, Y. Chang, R. Wang, Z. Wang, G. Li, D. Zhu and M. R. Bryce, *Dalton Trans.*, 2022, **51**, 16119-16125.

4 J. Yang, Q. Cao, L. Hao, G. G. Yang, W. L. Hu, L. N. Ji and Z. W. Mao, *Chem. Commun.*, 2018, **54**, 271-274.

5 D. R. Martir, C. Momblona, A. Pertegás, D. B. Cordes, A. M. Z. Slawin, H. J. Bolink and E. Zysman-Colman, *ACS Appl. Mater. Interfaces*, 2016, **8**, 33907-33915.

6 H. U. Kim, S. Sohn, W. Choi, M. Kim, S. U. Ryu, T. Park, S. Jung and K. S. Bejoymohandas, *J. Mater. Chem. C*, 2018, **6**, 10640-10658.

7 G. Li, X. Ren, G. Shan, W. Che, D. Zhu, L. Yan, Z. Su and M. R. Bryce, *Chem. Commun.*, 2015, **51**, 13036-13039.

8 G. Li, S. Shi, Y. Gao, D. Zhu and Z. Su, *J. Organomet. Chem.*, 2021, **931**, 121628.

9 C. You, D. Liu, L. Wang, W. Zheng, M. Li, P. Wang and W. Zhu, *Chem. Eng. J.*, 2023, **452** 138956.

10 J. Zhao, Y. Gao, R. Huang, C. Chi, Y. Sun, G. Xu, X. H. Xia and S. Gou, *J. Am. Chem. Soc.*, 2023, **145**, 11633-11642.